

Analysis of BOSS Galaxy Data with Weighted Skew-Spectra

Shu-Fan Chen¹, Priyesh Chakraborty², and Cora Dvorkin³

Department of Physics, Harvard University, 17 Oxford Street, Cambridge, MA 02138, USA

E-mail: [1shufan_chen@g.harvard.edu](mailto:shufan_chen@g.harvard.edu), [2pchakraborty@g.harvard.edu](mailto:pchakraborty@g.harvard.edu),
[3cdvorkin@g.harvard.edu](mailto:cdvorkin@g.harvard.edu),

Abstract. We present the first application of the weighted skew-spectra to analyze non-Gaussian information in galaxy survey data. Using the tree-level galaxy skew-spectra together with the one-loop power spectrum multipoles, we analyze the Sloan Digital Sky Survey (SDSS)-III Baryon Oscillation Spectroscopic Survey (BOSS) galaxy clustering data, and target our search towards the equilateral bispectrum shape of primordial non-Gaussianity. We use the Effective Field Theory model for the galaxy power spectrum and bispectrum, and account for systematic effects, such as the survey geometry. From our likelihood analysis, we find $f_{\text{NL}}^{\text{equil}} = -34_{-334}^{+296}$ at 68% CL, consistent with previous works, while systematic errors from our treatment of the survey geometry lead to an unreliable estimation of $f_{\text{NL}}^{\text{ortho}}$. We further constrain the bias and counterterm parameters, while keeping the cosmology fixed to *Planck* 2018 values. As a check, we also validate our analysis pipeline using the *Nseries* simulation suite.

Contents

1	Introduction	1
2	The Theory Model	3
2.1	Primordial Bispectrum	4
2.2	Late-Time Power Spectrum and Bispectrum	4
2.3	Alcock-Paczynski Effect	7
2.4	Survey Geometry	8
2.5	Skew-Spectrum	9
3	The Data	10
3.1	Galaxy Catalogues	10
3.2	Estimation of Power Spectra and Skew-Spectra	12
4	Parameter Inference	14
4.1	Likelihood Function	14
4.2	Parameters and Prior Choices	15
5	Results and Discussions	16
6	Conclusions	19
A	BAO Damping	22
B	Survey Geometry Approximation	22

1 Introduction

We have learned from precision cosmological measurements that our model of the universe at large scales can be described by a few parameters. However, the physics of the early universe remains to be fully elucidated. One interesting observable that can be used to learn about this period is primordial non-Gaussianity (PNG), which is a weak deviation from a pure Gaussian probability distribution function of matter and radiation fluctuations in the early universe. Such a signal could be generated by interactions during an early period of inflation, and therefore a detection of PNG could additionally provide a window into probing physics at unprecedented energy scales [1–4].

The simplest model of inflation, featuring a single field, can be captured by the so called Effective Field Theory (EFT) of inflation [5], which produces two dominant types of primordial bispectra. One is the equilateral shape, which peaks when the wavenumbers of the fluctuations, k_1 , k_2 , and k_3 , satisfy $k_1 \sim k_2 \sim k_3$, and the other one is the orthogonal shape which peaks in the flattened configuration ($k_1 \sim k_2 \sim k_3/2$). Their amplitudes are parametrized by $f_{\text{NL}}^{\text{equil}}$ and $f_{\text{NL}}^{\text{ortho}}$, respectively.

The leading constraints on $f_{\text{NL}}^{\text{equil}}$ and $f_{\text{NL}}^{\text{ortho}}$ have thus far been obtained through cosmic microwave background (CMB) observations. The *Planck* 2018 satellite provided us with measurements of $f_{\text{NL}}^{\text{equil}} = -26 \pm 47$ and $f_{\text{NL}}^{\text{ortho}} = -38 \pm 24$ at 68% CL [6]. It is expected that CMB constraints will be improved with the advent of upcoming large-scale structure (LSS) surveys, which in principle contain orders of magnitude more modes of information [7]. The search for PNG in the Sloan Digital Sky Survey (SDSS)-III Baryon Oscillation Spectroscopic Survey (BOSS) catalogue [8, 9] has already begun [10–15], and while the status is not currently at a competitive level with the CMB, these constraints are expected to improve with upcoming galaxy surveys such as DESI [16], the Vera Rubin Observatory [17], SPHEREx [18], and EUCLID [19], among others.

A standard route for constraining PNG has been by using the galaxy bispectrum. A challenge with this approach is that estimating this statistic from a survey or mock is computationally expensive. Since the covariance matrix is typically needed to be estimated from many ($\mathcal{O}(1000)$) mock catalogs, performing a Markov Chain Monte Carlo (MCMC) likelihood analysis can prove to be a time-consuming task. To circumvent this issue, the bispectrum weighted skew-spectrum (henceforth skew-spectrum) was introduced as a tool in LSS analyses as a compression of the bispectrum [20]. The skew-spectrum is obtained by averaging over the bispectrum using an appropriate kernel, so that the process of estimating it from data reduces to factorizable convolutions, which can all be reduced to a sequence of Fast Fourier Transforms (FFTs). This type of method was initially developed in order to expedite estimators of f_{NL} from CMB temperature and polarization data [21], and has been subsequently developed for the large-scale structure of the universe. Refs. [20, 22] studied such skew-spectra for the galaxy bispectrum in Fourier space, and these were subsequently extended to redshift-space bispectra [23, 24] and harmonic space for weak-lensing analyses [25, 26]. In this paper, we present the first application of skew-spectra to LSS data.

Using the BOSS DR12 galaxy catalogue [8, 9], we focus on investigating PNG due to single-field inflation using the one-loop galaxy power spectrum multipoles and the tree-level galaxy skew-spectra. There are some differences in the precise redshift-space distortions (RSD) information used in the literature and the one we employ here. Ref. [10] makes use of the bispectrum monopole at tree-level and uses the window-free estimator [6] in order to decontaminate the measured bispectrum from survey geometry effects. Ref. [12] goes to 1-loop order in the bispectrum monopole and, instead, chooses to approximate window function effects using a phenomenological approximation [27]. In this work, we will use skew-spectra with multiple kernels to capture RSD information in the bispectrum, and we will apply a phenomenological approximation to the window effects.

The outline of this work is as follows: we first present the theoretical specifications of our model for the power and skew-spectra in §2, which uses the Effective Field Theory of large-scale structure framework. The estimation of skew-spectra from the BOSS galaxy catalogues and from simulations is discussed in §3, and details regarding our inference methodology are provided in §4. Finally, we discuss our results in §5.

2 The Theory Model

One of the main advantages of the skew-spectra is to optimally measure the amplitude parameters in the galaxy bispectrum, while being computationally much more efficient than the standard bispectrum. The amplitude A_B of the galaxy bispectrum $B_g(\mathbf{k}_1, \mathbf{k}_2, \mathbf{k}_3)$ is obtained through a minimum-variance estimator [20, 28],

$$\hat{A}_B = \int \frac{d^3k}{N_{\text{th}}} \int_{\mathbf{q}} \frac{B_g^{\text{th}}(\mathbf{k}, \mathbf{q}, -\mathbf{k} - \mathbf{q})}{P_{gg}(k)P_{gg}(q)P_{gg}(|\mathbf{k} + \mathbf{q}|)} \times [\delta_g(\mathbf{k})\delta_g(\mathbf{q})\delta_g(-\mathbf{k} - \mathbf{q}) - 3\langle\delta_g(\mathbf{k})\delta_g(\mathbf{q})\rangle\delta_g(-\mathbf{k} - \mathbf{q})], \quad (2.1)$$

where $B_g^{\text{th}}(\mathbf{k}_1, \mathbf{k}_2, \mathbf{k}_3)$ is the theoretical template for the galaxy bispectrum, $P_{gg}(k)$ is the galaxy power spectrum, and N_{th} is the number of k -modes. Hereafter, we will use the following notation: $\int_{\mathbf{q}} \equiv \int \frac{d^3q}{(2\pi)^3}$.

The amplitude estimator is a sum of the form $\hat{A}_B = \hat{A}_B^{(1)} + \hat{A}_B^{(3)}$, where $\hat{A}_B^{(1)}$ is a linear term in $\delta_g(\mathbf{k})$ and $\hat{A}_B^{(3)}$ is cubic in $\delta_g(\mathbf{k})$ [29]. We will ignore the linear term, which only has the effect of increasing the variance. To reduce clutter, we will still call the amplitude estimator \hat{A}_B (instead of $\hat{A}_B^{(3)}$).

If the theoretical bispectrum can be written in a separable fashion, i.e. $B_g^{\text{th}}(\mathbf{k}_1, \mathbf{k}_2, \mathbf{k}_3) = f(\mathbf{k}_1)g(\mathbf{k}_2)h(\mathbf{k}_3)$, the above estimator can be rewritten as:

$$\begin{aligned} \hat{A}_B &= \int \frac{d^3k}{N_{\text{th}}} \left[\frac{f\delta_g}{P_{gg}} \star \frac{g\delta_g}{P_{gg}} \right] (\mathbf{k}) \frac{h\delta_g}{P_{gg}}(-\mathbf{k}) \\ &= 4\pi \int \frac{dk k^2}{N_{\text{th}}} \hat{P}(k), \end{aligned} \quad (2.2)$$

where $\hat{P}(k)$ is the skew-spectrum defined as:

$$\hat{P}(k) = \int \frac{d\hat{\mathbf{k}}}{4\pi} \left[\frac{f\delta_g}{P_{gg}} \star \frac{g\delta_g}{P_{gg}} \right] (\mathbf{k}) \frac{h\delta_g}{P_{gg}}(-\mathbf{k}). \quad (2.3)$$

We can relax the optimality of this statistic and, instead of B_g^{th} , choose any kernel $\mathcal{S}(\mathbf{k}, \mathbf{k}')$ to convolve with, as long as the kernel is still product separable. To be precise, given an arbitrary kernel $\mathcal{S}(\mathbf{k}, \mathbf{k}') = f(\mathbf{k})g(\mathbf{k}')h(-\mathbf{k} - \mathbf{k}')$, the estimator is defined as,

$$\hat{P}_{\mathcal{S}}(k) = \int \frac{d\hat{\mathbf{k}}}{4\pi} [f\delta_g \star g\delta_g] (\mathbf{k}) h\delta_g(-\mathbf{k}). \quad (2.4)$$

We will specify our choices for these kernels in §2.5. Note that given some arbitrary separable kernel \mathcal{S} , we can write the theory skew-spectrum as:

$$\begin{aligned} \tilde{P}_{\mathcal{S}}(k) &= \langle \hat{P}_{\mathcal{S}}(k) \rangle \\ &= \int \frac{d\hat{\mathbf{k}}}{4\pi} \int_{\mathbf{q}} \mathcal{S}(\mathbf{q}, \mathbf{k} - \mathbf{q}) B_g(\mathbf{q}, \mathbf{k} - \mathbf{q}, -\mathbf{k}), \end{aligned} \quad (2.5)$$

where B_g is the theoretical template for the galaxy bispectrum.

Therefore, in order to compute the skew-spectrum, it is necessary to first specify a theoretical model for the power spectrum and bispectrum. We will begin with a discussion of the primordial bispectrum shapes in §2.1, and then lay out the details of the late-time galaxy power spectrum and bispectrum, under the EFT of LSS in §2.2.

2.1 Primordial Bispectrum

By treating the inflaton field as a Goldstone mode of broken time-diffeomorphisms, the EFT of inflation generates interactions that are fixed by a few unknown speed-of-sound parameters [5, 10]. In this minimal scenario, the two cubic self-interactions of the inflaton field lead to two distinct shapes of bispectra, namely the equilateral and orthogonal shapes, with amplitudes $f_{\text{NL}}^{\text{equil}}$ and $f_{\text{NL}}^{\text{ortho}}$, respectively. The precise expression for the bispectrum of the primordial curvature perturbation ζ is given by [30, 31]:

$$B_{\zeta}(k_1, k_2, k_3) = \frac{18}{5} \Delta_{\zeta}^4 \frac{\mathcal{B}(k_1, k_2, k_3)}{k_1^2 k_2^2 k_3^2}. \quad (2.6)$$

Here $\Delta_{\zeta}^2 \approx 4.1 \times 10^{-8}$ [32] is the amplitude of the primordial power spectrum, i.e. $k^3 P_{\zeta}(k) = \Delta_{\zeta}^2 (k/k_*)^{n_s-1}$, where n_s is the spectral tilt and the pivot scale $k_* = 0.05 \text{ Mpc}^{-1}$. The equilateral and orthogonal templates fix the shape function \mathcal{B} , given by:

$$\mathcal{B}_{\text{equil}}(k_1, k_2, k_3) = \left(\frac{k_1}{k_2} + 5 \text{ perms.} \right) - \left(\frac{k_1^2}{k_2 k_3} + 2 \text{ perms.} \right) - 2, \quad (2.7)$$

$$\mathcal{B}_{\text{ortho}}(k_1, k_2, k_3) = (1+p) \frac{\Delta}{e_3} - p \frac{\Gamma^3}{e_3^2}. \quad (2.8)$$

The various parameters appearing above are defined as:

$$p = 8.52587, \quad \Delta = (-k_1 + k_2 + k_3)(k_1 - k_2 + k_3)(k_1 + k_2 - k_3) \quad (2.9)$$

$$e_2 = k_1 k_2 + k_2 k_3 + k_1 k_3, \quad e_3 = k_1 k_2 k_3 \quad (2.10)$$

$$\Gamma = \frac{2}{3} e_2 - \frac{1}{3} (k_1^2 + k_2^2 + k_3^2). \quad (2.11)$$

In the subsection below, we will discuss how these primordial shapes enter the late-time galaxy correlators.

2.2 Late-Time Power Spectrum and Bispectrum

The EFT of LSS is a perturbative model built to capture the gravitational evolution of galaxy correlators up to some nonlinear scale. It identifies an ultraviolet scale and provides a systematic method of including counterterms in order to appropriately renormalize the final correlators [33, 34].

The power spectrum and bispectrum of the density field δ_L in linear theory are given by:

$$\langle \delta_L(z, \mathbf{k}) \delta_L(z, \mathbf{k}') \rangle = (2\pi)^3 \delta_D(\mathbf{k} + \mathbf{k}') P_L(z, k) \quad (2.12)$$

$$\langle \delta_L(z, \mathbf{k}_1) \delta_L(z, \mathbf{k}_2) \delta_L(z, \mathbf{k}_3) \rangle = (2\pi)^3 \delta_D(\mathbf{k}_{123}) B_L(z; \mathbf{k}_1, \mathbf{k}_2, \mathbf{k}_3), \quad (2.13)$$

where the bispectrum B_L is determined by the primordial bispectrum B_ζ as:

$$B_L(z; \mathbf{k}_1, \mathbf{k}_2, \mathbf{k}_3) = f_{\text{NL}} T(z, k_1) T(z, k_2) T(z, k_3) B_\zeta(k_1, k_2, k_3). \quad (2.14)$$

Here, $\mathbf{k}_{123} \equiv \mathbf{k}_1 + \mathbf{k}_2 + \mathbf{k}_3$ (this notation will be followed henceforth) and $T(z, k) = \sqrt{P_L(z, k)/P_\zeta(k)}$ is the matter transfer function at a given redshift z .

Apart from the non-Gaussianities generated due to purely gravitational terms, we will also need to account for the non-linear response of the PNG to the late time power spectrum due to gravity. We follow the same EFT of LSS model described in Ref. [10]. The perturbation theory model we use in this work is consistent with the ones previously used in Refs. [35, 36]. We include the effects of redshift-space distortion (RSD), Fingers-of-God (FoG) [37, 38], infrared (IR) resummation [39–41], along with the appropriate counterterms at the corresponding order of perturbation theory. We rely on the publicly available code CLASS-PT¹[42], an extension of the CLASS² [43] Boltzmann code, in order to obtain the galaxy power spectrum.

Under the EFT of LSS framework, the perturbative expansion of galaxy density fluctuations in terms of the linear matter fluctuations $\delta_L(k, z)$ takes the following form:

$$\begin{aligned} \delta_g(\mathbf{k}, z) &= Z_1(\mathbf{k})\delta_L(k, z) + \int_{\mathbf{q}} Z_2(\mathbf{q}, \mathbf{k} - \mathbf{q})\delta_L(\mathbf{q}, z)\delta_L(\mathbf{k} - \mathbf{q}, z) \\ &+ \int_{\mathbf{q}_1, \mathbf{q}_2, \mathbf{q}_3} (2\pi)^3 \delta_D(\mathbf{q}_{123} - \mathbf{k}) Z_3(\mathbf{q}_1, \mathbf{q}_2, \mathbf{q}_3)\delta_L(\mathbf{q}_1, z)\delta_L(\mathbf{q}_2, z)\delta_L(\mathbf{q}_3, z) \\ &+ f_{\text{NL}} b_\zeta \frac{k^2}{k_{\text{NL}}^2} \frac{\delta_L(\mathbf{k}, z)}{T(k, z)} + \delta_{\text{ctr}}(\mathbf{k}, z), \end{aligned} \quad (2.15)$$

Here, k_{NL} is the non-linear scale for matter fluctuations, which is redshift-dependent in general. To avoid clutter, we will be omitting the redshift z for the transfer function and the density field from now on. The RSD kernels are given by:

$$\begin{aligned} Z_1(\mathbf{k}) &= b_1 + f\mu^2 \quad (2.16) \\ Z_2(\mathbf{k}_1, \mathbf{k}_2) &= b_1 F_2(\mathbf{k}_1, \mathbf{k}_2) + \frac{b_2}{2} + b_{\mathcal{G}_2} S^2(\mathbf{k}_1, \mathbf{k}_2) + f\mu^2 G_2(\mathbf{k}_1, \mathbf{k}_2) \\ &+ \frac{f\mu k}{2} \left[\frac{\mu_1}{k_1} (b_1 + f\mu_2^2) + \frac{\mu_2}{k_2} (b_1 + f\mu_1^2) \right] \\ S^2(\mathbf{k}_1, \mathbf{k}_2) &= (\hat{\mathbf{k}}_1 \cdot \hat{\mathbf{k}}_2)^2 - 1, \end{aligned} \quad (2.17)$$

and $F_2(\mathbf{k}, \mathbf{k}')$ and $G_2(\mathbf{k}, \mathbf{k}')$ are the usual standard perturbation theory (SPT) kernels [44]. The expression for Z_3 can be found in Ref. [42]. Here, b_1 , b_2 and $b_{\mathcal{G}_2}$ are the galaxy bias parameters and f is the growth rate. The piece δ_{ctr} contains all the required counterterm operators, which we will specify later. Lastly, the $f_{\text{NL}} b_\zeta$ term is the so-called scale-dependent bias term [45, 46].

Using the ingredients above, we can write the galaxy power spectrum as:

$$\begin{aligned} P_{gg}(k, \mu) &= P_{gg,L}(k, \mu) + P_{gg,\text{PNG-bias}}(k, \mu) + P_{gg,1L}(k, \mu) \\ &+ P_{gg,\text{ctr}}(k, \mu) + P_{\text{stoch}}(k, \mu). \end{aligned} \quad (2.18)$$

¹<https://github.com/Michalychforever/CLASS-PT>

²https://lesgourg.github.io/class_public/class.html

The linear piece $P_{gg,L}$ is the linear RSD power spectrum, which includes the damping of the baryon acoustic oscillation (BAO) feature and captures the IR resummation [41]. The term $P_{gg,1L}$ contains the standard perturbation theory (SPT) 1-loop piece, as well as the non-Gaussian loop integral due to PNG [10]:

$$P_{gg,1L}(k, \mu) = P_{gg,1L,SPT}(k, \mu) + 2Z_1(\mathbf{k}) \int_{\mathbf{q}} Z_2(\mathbf{q}, \mathbf{k} - \mathbf{q}) B_L(\mathbf{q}, \mathbf{k} - \mathbf{q}, -\mathbf{k}). \quad (2.19)$$

Details about the 1-loop SPT term can be found in Ref. [42]. The term $P_{gg,PNG-bias}$ corresponds to the well known scale-dependent bias contribution:

$$P_{gg,PNG-bias}(k, \mu) = \frac{2f_{NL}b_{\zeta}Z_1(\mathbf{k})k^2}{k_{NL}^2} \frac{P_L(k)}{T(k)}. \quad (2.20)$$

Next, we have the counterterm contribution, $P_{gg,ctr}$, that captures short-distance effects, and it is given by [38]:

$$P_{gg,ctr}(k, \mu) = [\tilde{c}_0 + \tilde{c}_2 f \mu^2 + \tilde{c}_4 f^2 \mu^4] k^2 P_L(k) - \tilde{c} f^4 \mu^4 k^4 (b_1 + f \mu^2)^2 P_L(k), \quad (2.21)$$

where $\{\tilde{c}_0, \tilde{c}_2, \tilde{c}_4, \tilde{c}\}$ are free parameters to be fit from the data. Finally, there is a stochastic shot-noise contribution to the power spectrum given by:

$$P_{stoch}(k, \mu) = \frac{1}{\bar{n}} \left[1 + P_{shot} + a_0 \left(\frac{k}{k_{NL}} \right)^2 + a_2 \mu^2 \left(\frac{k}{k_{NL}} \right)^2 \right]. \quad (2.22)$$

Here, $\{P_{shot}, a_0, a_2\}$ are free parameters as well, and should be included in order to account for non-Poissonian features such as exclusion effects and fiber collisions in the shot-noise. With all these pieces, the power spectrum multipoles are defined as:

$$P_{gg,\ell}(k) = \frac{2\ell + 1}{2} \int_{-1}^1 d\mu \mathcal{L}_{\ell}(\mu) P_{gg}(k, \mu), \quad (2.23)$$

where $\mathcal{L}_{\ell}(\mu)$ is the Legendre polynomial of order ℓ .

The bispectrum, in contrast, is more straightforward since we work at linear order in SPT:

$$B_g(\mathbf{k}_1, \mathbf{k}_2, \mathbf{k}_3) = B_{g,G}(\mathbf{k}_1, \mathbf{k}_2, \mathbf{k}_3) + Z_1(\mathbf{k}_1) Z_1(\mathbf{k}_2) Z_1(\mathbf{k}_3) B_L(\mathbf{k}_1, \mathbf{k}_2, \mathbf{k}_3) \quad (2.24)$$

$$B_{g,G}(\mathbf{k}_1, \mathbf{k}_2, \mathbf{k}_3) = 2Z_2(\mathbf{k}_1, \mathbf{k}_2) Z_1(\mathbf{k}_1) Z_1(\mathbf{k}_2) P_L(k_1) P_L(k_2) + 2 \text{ perms.}, \quad (2.25)$$

where $B_{g,G}$ is the galaxy bispectrum from the Gaussian initial condition. Although our bispectrum is only at tree-level, following Ref. [36], we choose to include separate counterterms in order to capture the FoG effects [36–38]. This can be taken care of by modifying the Z_1 kernel in Eq. (2.24) to

$$\begin{aligned} Z_1(\mathbf{k}) &\rightarrow Z_1^{\text{FoG}}(\mathbf{k}) \\ &= (b_1 + f \mu^2 - c_0^B k^2 - c_1^B k^2 \mu^2 - c_2^B k^2 \mu^4), \end{aligned} \quad (2.26)$$

where $\{c_0^B, c_1^B, c_2^B\}$ are additional free parameters³. The shot-noise contribution to the bispectrum can be written as:

$$B_{\text{stoch}}(\mathbf{k}_1, \mathbf{k}_2, \mathbf{k}_3) = \frac{B_{\text{shot}}}{\bar{n}} [Z_1(\mathbf{k}_1) b_1 P_L(k_1) + 2 \text{ perms.}] + \frac{1 + P_{\text{shot}}}{\bar{n}} [2Z_1(\mathbf{k}_1) f \mu_1^2 P_L(k_1) + 2 \text{ perms.}] + \frac{1 + A_{\text{shot}}}{\bar{n}^2}, \quad (2.27)$$

where A_{shot} and B_{shot} are additional free parameters that measure the deviation from the Poisson prediction, which we must fit from the data. Lastly, to include the BAO damping, we approximate it by making the substitution $P_L(k) \rightarrow P_{L,\text{IR}}(k)$ in all of the expressions above, i.e. the damping is included at the level of the linear matter power spectrum [12]. We provide details about this procedure in Appendix A.

2.3 Alcock-Paczynski Effect

The coordinate transformation from redshift space to physical distance relies on the assumption of a fiducial cosmology. For us, that corresponds to the following choice of fiducial parameters: $\Omega_m = 0.31$ and $h = 0.676$ [47]. As a result, we need to perform an Alcock-Paczynski correction [48] in order to make the coordinate system consistent between the observation and the theory. Following the analysis in Ref. [12], we account for the Alcock-Paczynski effect only at the tree-level, as it is estimated to be negligible at the one-loop level.

First, let us define the dilation parameters [42, 49]:

$$\begin{aligned} \alpha_{\parallel}(z) &= \frac{H^{\text{fid}}(z)}{H(z)}, \\ \alpha_{\perp}(z) &= \frac{D_A(z)}{D_A^{\text{fid}}(z)}, \end{aligned} \quad (2.28)$$

where $D_A(z)$ is the angular diameter distance to redshift z . If we set $F = \alpha_{\parallel}/\alpha_{\perp}$, then we can write the observed bispectrum and power spectrum in terms of the ones computed using the fiducial cosmology as:

$$\begin{aligned} B_g^{\text{obs}}(\tilde{k}_1, \tilde{k}_2, \tilde{k}_3, \tilde{\mu}_1, \tilde{\mu}_2) &= \frac{1}{\alpha_{\parallel}^2 \alpha_{\perp}^4} B_g(k_1, k_2, k_3, \mu_1, \mu_2), \\ P_{gg}^{\text{obs}}(\tilde{k}, \tilde{\mu}) &= \frac{1}{\alpha_{\parallel} \alpha_{\perp}^2} P_{gg}(k, \mu), \end{aligned} \quad (2.29)$$

where k and μ refer to the fiducial cosmology, and \tilde{k} and $\tilde{\mu}$ refer to the observed cosmology, and they are related through the following relation:

$$\begin{aligned} k &= \frac{\tilde{k}}{\alpha_{\perp}} [1 + \tilde{\mu}^2 (F^{-2} - 1)]^{1/2}, \\ \mu &= \frac{\tilde{\mu}}{F} [1 + \tilde{\mu}^2 (F^{-2} - 1)]^{-1/2}. \end{aligned} \quad (2.30)$$

³Note that we use different counterterms in the bispectrum, although they correspond to the same operators as those that appear in $P_{gg}(k, \mu)$. This is because the counterterms in the power spectrum renormalize the loop-correction in addition to capturing the FoG effect. Since we work at linear order only in the bispectrum, only the FoG effects need to be captured. We thank O. Philcox for clarification regarding this point.

2.4 Survey Geometry

Due to the non-trivial survey geometry, the theory power spectrum and bispectrum must be appropriately convolved with the survey window function in order to match the one measured from the data. Here we outline the procedure that we follow to account for the survey geometry for the power spectrum multipoles and the bispectrum shapes.

The window convolution for the power spectrum can be streamlined by working with the two-point correlation function, computed using Hankel transforms [47, 50]. That is, if we have the unconvolved power spectrum multipoles $P_\ell^{\text{unconv}}(k)$, we can first compute the Hankel transform⁴ to obtain the two-point correlation function multipoles $\xi_\ell(r)$, and then convolve them with the window function multipoles $W_\ell(r)$ ⁵ to get $\hat{\xi}_\ell(r)$:

$$\hat{\xi}_0(r) = \xi_0(r)W_0(r)^2 + \frac{1}{5}\xi_2(r)W_2(r)^2 + \frac{1}{9}\xi_4(r)W_4(r)^2 \quad (2.31)$$

$$\begin{aligned} \hat{\xi}_2(r) = & \xi_0(r)W_2(r)^2 + \xi_2(r) \left[W_0(r)^2 + \frac{2}{7}W_2(r)^2 + \frac{2}{7}W_4(r)^2 \right] \\ & + \xi_4(r) \left[\frac{2}{7}W_2(r)^2 + \frac{100}{693}W_4(r)^2 \right] \end{aligned} \quad (2.32)$$

$$\begin{aligned} \hat{\xi}_4(r) = & \xi_0(r)W_4(r)^2 + \xi_2(r) \left[\frac{18}{35}W_2(r)^2 + \frac{20}{77}W_4(r)^2 \right] \\ & + \xi_4(r) \left[W_0(r)^2 + \frac{20}{77}W_2(r)^2 + \frac{162}{1001}W_4(r)^2 \right]. \end{aligned} \quad (2.33)$$

Finally, the window-convolved power spectrum multipoles $P_\ell^{\text{conv}}(k)$ can be obtained by performing the inverse Hankel transform with $\hat{\xi}_\ell(r)$:

$$P_\ell^{\text{conv}}(k) = 4\pi(-i)^\ell \int dr r^2 \hat{\xi}_\ell(r) j_\ell(kr). \quad (2.34)$$

Due to convergence issues with the Hankel transform, this procedure must be modified slightly if $P_\ell(k)$ is at one-loop order instead, or does not decay sufficiently fast at large k . We artificially extrapolate the power spectra at high k ($k \geq 0.5 \text{ hMpc}^{-1}$) to be proportional to k^{-4} , so that the Hankel transform converges.

In the bispectrum case, directly convolving with the window function is more computationally expensive. To overcome this issue, we use an approximate method following Refs. [27, 49]. Suppose the functional form of the galaxy bispectrum is a product of two matter power spectra and a function of wavenumbers \mathbf{k} ,

$$B_g(\mathbf{k}_1, \mathbf{k}_2, \mathbf{k}_3) = P_L(k_1)P_L(k_2)\mathcal{Q}(\mathbf{k}_1, \mathbf{k}_2, \mathbf{k}_3) + 2 \text{ perms.}, \quad (2.35)$$

then the window-convolved bispectrum can be approximated as:

$$\begin{aligned} & \int_{\mathbf{k}', \mathbf{k}''} B_g(\mathbf{k}', \mathbf{k}'', -\mathbf{k}' - \mathbf{k}'') W_3(\mathbf{k}_1 - \mathbf{k}', \mathbf{k}_2 - \mathbf{k}'') \\ & \approx [P_L \star W](\mathbf{k}_1) [P_L \star W](\mathbf{k}_2) \mathcal{Q}(\mathbf{k}_1, \mathbf{k}_2, \mathbf{k}_3) + 2 \text{ perms.}, \end{aligned} \quad (2.36)$$

⁴The Hankel transforms are performed with `hank1`[51] using the FFTLog algorithm [52]. This can be found at <https://hank1.readthedocs.io/en/latest/>.

⁵The $W_\ell(r)$ s are publicly available at <https://www.ub.edu/bispectrum/page11.html> for the BOSS/Patchy [CMASS, LOWZ]×[NGC, SGC] simulations, as well as the ones for `Nseries` simulations.

where $W_3(\mathbf{k}_1, \mathbf{k}_2) \equiv \frac{1}{I_{33}} m(\mathbf{k}_1) m(\mathbf{k}_2) m^*(\mathbf{k}_1 + \mathbf{k}_2)$, $W(\mathbf{k}) = \frac{1}{I_{22}} |m(\mathbf{k})|^2$, $m(\mathbf{k})$ is the Fourier transform of the mask, and the normalization factors I_{22} and I_{33} will be precisely defined in §3.1 [27]. The notation $P_L \star W$ denotes the window convolution applied to the power spectrum, as discussed previously in this section. This approximation is valid for modes that are not comparable to the survey geometry. For wavenumbers $\gtrsim 0.03 h\text{Mpc}^{-1}$, the error of the approximation is less than 5%, with only 1% differences on parameter estimation using modes between 0.03 to 0.15 $h\text{Mpc}^{-1}$ [27]. Following Ref. [12] we employ a similar approximation to convolve the primordial piece:

$$\begin{aligned} B_L(\mathbf{k}_1, \mathbf{k}_2, \mathbf{k}_3) &= \frac{1}{3} \left(\frac{B_L(\mathbf{k}_1, \mathbf{k}_2, \mathbf{k}_3)}{P_L(k_1)P_L(k_2)} P_L(k_1)P_L(k_2) + 2 \text{ perms.} \right) \\ &\rightarrow \frac{1}{3} \left(\frac{B_L(\mathbf{k}_1, \mathbf{k}_2, \mathbf{k}_3)}{P_L(k_1)P_L(k_2)} (W \star P_L)(\mathbf{k}_1)(W \star P_L)(\mathbf{k}_2) + 2 \text{ perms.} \right). \end{aligned} \quad (2.37)$$

We find that the error due to this approximation, across all skew-spectra, is at most 6% for the equilateral shape and 18% for the orthogonal shape. Details regarding these estimates can be found in Appendix B. We will further assess the goodness of this approximation through a validation test of our pipeline on the `Nseries` simulations in §5.

2.5 Skew-Spectrum

In this section, we will describe the formalism of the skew-spectra used in our analysis of the BOSS data. In order to obtain the theory skew-spectrum, we must specify the kernels used, $\mathcal{S}(\mathbf{k}, \mathbf{k}')$. From our previous work [26], we know that the Legendre polynomial kernels can preserve much of the information from the full bispectrum analysis and, therefore, these will be our baseline kernels. In addition, we will add the primordial non-Gaussianity shapes for both equilateral and orthogonal as extra kernels. To sum up, our skew-spectra are defined as follows:

$$\tilde{P}_{S_i}(k) = \int \frac{d\mathbf{k}}{4\pi} \int_{\mathbf{q}} \mathcal{S}_i(\mathbf{q}, \mathbf{k} - \mathbf{q}) B_g(\mathbf{q}, \mathbf{k} - \mathbf{q}, -\mathbf{k}), \quad (2.38)$$

with kernels \mathcal{S}_i given by:

$$\mathcal{S}_1 = 1 \quad (2.39)$$

$$\mathcal{S}_2 = \frac{1}{2} \left(\frac{k_1}{k_2} + \frac{k_2}{k_1} \right) \frac{\mathbf{k}_1 \cdot \mathbf{k}_2}{k_1 k_2} \quad (2.40)$$

$$\mathcal{S}_3 = \frac{1}{2} \left[3 \left(\frac{\mathbf{k}_1 \cdot \mathbf{k}_2}{k_1 k_2} \right)^2 - 1 \right] \quad (2.41)$$

$$\mathcal{S}_{\text{equil}} = T(k_1)T(k_2)T(k_3) \Delta_\zeta^4 \frac{\mathcal{B}_{\text{equil}}(k_1, k_2, k_3)}{k_1^2 k_2^2 k_3^2} \times \frac{1}{P_L(k_1)P_L(k_2)} \quad (2.42)$$

$$\mathcal{S}_{\text{ortho}} = T(k_1)T(k_2)T(k_3) \Delta_\zeta^4 \frac{\mathcal{B}_{\text{ortho}}(k_1, k_2, k_3)}{k_1^2 k_2^2 k_3^2} \times \frac{1}{P_L(k_1)P_L(k_2)}. \quad (2.43)$$

In order to perform the integral in Eq. (2.38), we choose the following coordinate system [23]:

$$\hat{\mathbf{z}} = (0, 0, 1), \quad \hat{\mathbf{k}} = \left(0, \sqrt{1 - \mu_k^2}, \mu_k\right), \quad \hat{\mathbf{q}} = \left(\sqrt{1 - \mu_q^2} \cos \phi_q, \sqrt{1 - \mu_q^2} \sin \phi_q, \mu_q\right), \quad (2.44)$$

where $\mu_k = \hat{\mathbf{k}} \cdot \hat{\mathbf{z}}$, $\mu_q = \hat{\mathbf{q}} \cdot \hat{\mathbf{z}}$, $\cos(\phi_q) = \hat{\mathbf{q}} \cdot \hat{\mathbf{x}}$, and $\hat{\mathbf{z}}$ is the line-of-sight direction. We use the publicly available package `pycuba`⁶ [53, 54] to numerically evaluate the resulting 4-dimensional integral. The skew-spectrum computed from the data is averaged over a spherical shell in Fourier space. To mimic this, the theoretical skew-spectrum \tilde{P}_{S_j} is computed at the i^{th} -bin Δ_i as:

$$\tilde{P}_{S_j}(k_{\text{eff},i}) = \frac{\sum_{k \in \Delta_i} k \tilde{P}_{S_j}(k)}{\sum_{k \in \Delta_i} k}, \quad (2.45)$$

with $k_{\text{eff},i} = (\sum_{k \in \Delta_i} k^2) / (\sum_{k \in \Delta_i} k)$ being the effective wavenumber.

3 The Data

In this section, we will specify the details of our primary dataset, the 12th data release (DR12) of the BOSS survey. We further use two simulation suites, the `MultiDark-Patchy` and the `Nseries` mocks for covariance estimation and validation, respectively. Finally, we will discuss the estimation of the skew-spectra from the data.

3.1 Galaxy Catalogues

We use three different galaxy catalogues in our analysis: BOSS DR12 [55], `MultiDark-Patchy`⁷ (hereafter, “Patchy mocks”) and `Nseries` mocks⁸ [9, 58]. The data are broken down into two patches of the sky: the northern galactic cap (NGC) and the southern galactic cap (SGC). Further, the redshift range is cut into the redshift ranges z_{CMASS} and z_{LOWZ} :

$$\begin{aligned} z_{\text{CMASS}} &= [0.43, 0.70] \text{ with } z_{\text{eff}} = 0.57, \\ z_{\text{LOWZ}} &= [0.15, 0.43] \text{ with } z_{\text{eff}} = 0.32. \end{aligned} \quad (3.1)$$

The effective redshift z_{eff} for each range is used to paint the data onto a grid in redshift space, and also to compute the theory power spectra and skew-spectra. This turns out to be four different chunks of the sky in total for our full BOSS analysis. The survey window function is obtained via the public MANGLE mask⁹ [59]. We give here a brief summary of the catalogues that we use:

⁶`pycuba`, <https://github.com/JohannesBuchner/PyMultiNest/>, is a python wrapper for `cuba` [53] which provides four different routines to compute the numerical integral. We use the Divonne routine for most of the computation, and have checked that it agrees with other routines for the case considered here.

⁷The BOSS DR12 catalogues and `Patchy` simulations can be downloaded from <https://data.sdss.org/sas/dr12/boos/lss/>. [56, 57]. We use `CMASSLOWZTOT` for BOSS data in our analysis.

⁸The `Nseries` mocks can be found in <https://www.ub.edu/bispectrum/page11.html>.

⁹Available at <https://space.mit.edu/~molly/mangle/>.

	h	ω_b	ω_c	σ_8	n_s	$\sum m_\nu$ [eV]
<i>Planck</i> 2018	0.673	0.022	0.120	0.8120	0.966	0.06
Nseries mocks	0.700	0.023	0.117	0.8200	0.960	0.00
Patchy mocks	0.678	0.022	0.119	0.8288	0.960	0.00

Table 1. Fiducial cosmology for *Planck* 2018 data, Nseries and Patchy simulations.

- **BOSS DR12:** This is the primary catalogue that we use for parameter inference.
- **Patchy mocks:** A set of 2048 simulations from the “MultiDark-Patchy” suite, which is run using an approximate scheme. We use this set to obtain the covariance matrix for our likelihood function.
- **Nseries mocks:** We use this set of simulations to validate our analysis pipeline, as this set is a full N-body simulation unlike the approximate scheme applied in Patchy mocks. There are a total of 84 semi-independent mocks, created from different projections of seven independent N-body simulations. Each of these 84 boxes cover as much volume as the CMASS NGC sample.

The fiducial values of the cosmological parameters for Nseries and Patchy mocks are listed in Table 1, together with the *Planck* fiducial values, for comparison.

We apply the Feldman-Kaiser-Peacock estimator (FKP) [60] to estimate power spectrum multipoles and skew-spectra in our analysis. The FKP formalism aims to minimize the statistical error by giving a weight, $\omega_{\text{FKP}} = 1/(1+\bar{n}_g(z)P_{\text{FKP}})$, to each object in the catalogue, with $\bar{n}_g(z)$ being the number density of galaxies at redshift z . P_{FKP} is chosen to be the amplitude of the galaxy power spectrum where the signal is maximized. In our work, we set $P_{\text{FKP}} = 10^4 h^{-3} \text{Mpc}^3$, corresponding to $k = 0.10 h \text{Mpc}^{-1}$ for both BOSS data and Patchy mocks; while for Nseries mocks, we instead use the FKP weight provided in the public catalogue file. Additional weights ω_c are needed in order to capture observational effects. For BOSS data, we use $\omega_c = (\omega_{\text{rf}} + \omega_{\text{fc}} - 1)\omega_{\text{sys}}$ to capture redshift-failure, fiber collision and systematic effects [50]. For Patchy mocks, we use $\omega_c = \omega_{\text{veto}}\omega_{\text{fc}}$, for veto masks and fiber collisions. For Nseries mocks, we use ω_c directly provided in the catalogue file. The FKP-weighted field is then given by taking the difference between number densities of galaxies $n_g(\mathbf{r})$ and that of random particles $n_r(\mathbf{r})$:

$$F_\lambda(\mathbf{r}) = \frac{\omega_{\text{FKP}}(\mathbf{r})}{I_{\lambda\lambda}^{1/\lambda}} [\omega_c(\mathbf{r})n_g(\mathbf{r}) - \alpha n_r(\mathbf{r})], \quad (3.2)$$

where

$$I_{\lambda_1\lambda_2} = \int d^3\mathbf{r} \omega_{\text{FKP}}^{\lambda_1}(\mathbf{r}) \langle n_g \omega_c \rangle^{\lambda_2}(\mathbf{r}), \quad (3.3)$$

and α denotes the ratio of the number between galaxies and random particles. We choose random catalogues that are 50 times larger than the galaxy dataset/mocks, in order to capture the survey geometry as well as to reduce the additional shot-noise from these random particles. The λ in the above expression is an integer that depends on the spectra we are

interested in. For example, we have $\lambda = 2$ for the power spectrum and $\lambda = 3$ for the bispectrum. In our case, since the skew-spectrum is derived from the bispectrum, we will adopt $\lambda = 3$ for it.

To account for the survey geometry in the theory, we compute the window multipoles W_ℓ (see §2.4) from random catalogues, and normalize them appropriately so that $W_0(r \rightarrow 0) \rightarrow 1$. Physically, this is to ensure that the small-scale power spectrum and bispectrum are unaffected by the mask.

Particular care has to be taken in the normalization of the FKP field, i.e. the factor I_{22} , on the data side. The usual approximation for I_{22} involves summing over all the random particles, $I_{22}^{\text{approx}} \approx \alpha \sum_i \omega_{\text{FKP},i}^2 n_r(\mathbf{r}_i)$. However, it is known that this can result in roughly 10% of suppression on the amplitude of BOSS data, which leads to an incorrect estimation of σ_8 [61, 62]. In order to have consistent normalization between the data and the theoretical model, we do not use this approximation and instead perform the full random pair count with the code `Corrfunc` [63]¹⁰. The correct I_{22} can be evaluated with the random pair count (pc) as (see e.g. [64]):

$$I_{22}^{\text{pc}} = \frac{3\alpha^2 RR(\Delta)}{4\pi(r_{\text{max}}^3 - r_{\text{min}}^3)}, \quad (3.4)$$

where Δ is the r -bin centered at $1 h^{-1}\text{Mpc}$ with range being $[r_{\text{min}}, r_{\text{max}}]$ and $RR(r)$ is the random pair count including FKP weights with separation r . In the end, I_{22}^{pc} is used to ensure consistent normalization of window multipoles between data and theoretical modelling. Our computation agrees with the one shown in Ref. [61] for BOSS data, which split the redshift range into $z_1 = [0.2, 0.5]$ and $z_3 = [0.5, 0.75]$.

Finally, we embed the FKP field into a cubic box with length $3500 h^{-1}\text{Mpc}$ on each side for all the data and simulations we consider. We then apply the triangular-shaped cloud (TSC) scheme to generate a mesh with 512^3 pixels in total, which is equivalent to having a Nyquist wavenumber of $k_{\text{Nyq}} = 0.46 h\text{Mpc}^{-1}$. We also perform grid-deconvolution in Fourier space to correct aliasing from the mass assignment [65], that is, the way we assign each particle to a specific pixel.

3.2 Estimation of Power Spectra and Skew-Spectra

We compute the power spectrum multipoles $\hat{P}_\ell(k)$ with $\ell = 0, 2, 4$ assuming the Yamamoto approximation [66], which fixes the line-of-sight (LoS) direction to that of a single galaxy for each galaxy pair, as opposed to a single LoS for the whole survey. Note that the hat here denotes that the spectrum is estimated from data or simulations. To compute the power spectrum, we choose $[k_{\text{min}}^P, k_{\text{max}}^P] = [0.01, 0.22] h\text{Mpc}^{-1}$ with bin size $\Delta k^P = 0.0115 h\text{Mpc}^{-1}$ for both the data and the simulations.

The separability of the skew-spectra kernels enables us to expedite their estimation from the data. In particular, given a kernel that can be decomposed as $\mathcal{S}(\mathbf{q}_1, \mathbf{q}_2) = \sum_i f_i(\mathbf{q}_1)g_i(\mathbf{q}_2)h_i(-\mathbf{k})$

¹⁰<https://corrfunc.readthedocs.io/en/master/>

with $\mathbf{q}_1 + \mathbf{q}_2 = \mathbf{k}$, the skew-spectrum can be written as a sum:

$$\hat{P}_S(k) = \sum_i \int \frac{d\hat{\mathbf{k}}}{4\pi} [f_i F_3 * g_i F_3](\mathbf{k}) [h_i F_3](-\mathbf{k}), \quad (3.5)$$

where $F_3(\mathbf{r})$ is the FKP field defined in §3.1 with $\lambda = 3$. The convolution, being the most expensive part of the above expression, can easily be recasted into a sequence of FFTs by relying on the fact that convolution in Fourier space is a point-wise product in position space. Therefore, after we have the FKP density field on the grid, we can then compute the skew-spectra by following these steps:

- Transform the FKP field into Fourier space: $F_3(\mathbf{r}) \rightarrow F_3(\mathbf{k})$.
- Compute $f_i(\mathbf{k})F_3(\mathbf{k})$, $g_i(\mathbf{k})F_3(\mathbf{k})$ and $h_i(\mathbf{k})F_3(\mathbf{k})$ by point-wise products in Fourier space.
- Transform the data back to position space, and get $[f_i F_3](\mathbf{r})$, $[g_i F_3](\mathbf{r})$ and $[h_i F_3](\mathbf{r})$.
- Compute point-wise products between $[f_i F_3](\mathbf{r})$ and $[g_i F_3](\mathbf{r})$. This is equivalent to doing convolution in Fourier space and we denote it as $[f_i F_3 * g_i F_3](\mathbf{r})$.
- Compute the cross-correlation between $[f_i F_3 * g_i F_3](\mathbf{r})$ and $[h_i F_3](\mathbf{r})$ and sum over i , which runs over the components of the skew-spectrum, as shown in Eq. (3.5). We can then obtain the targeted skew-spectrum.

All the kernels for the skew-spectrum that we consider here are separable (see §2.5), and hence we can follow the above steps to expedite their computation. In order to estimate the skew-spectra from the data, we must specify two different ranges of k . The first range of k is the range in which we perform the convolution. We set this range to be $\mathcal{I}_{\text{conv}} = [k_{\text{conv,min}}^{\tilde{P}}, k_{\text{conv,max}}^{\tilde{P}}] = [0.03, 0.08] h\text{Mpc}^{-1}$, in which the density field lies within the linear regime. The choice of $k_{\text{conv,min}}^{\tilde{P}}$ also ensures that our approximation for the window convolution of the bispectrum (mentioned in §2.4) is within 5% error. The second range of k is the range over which we evaluate the cross-correlation between $[f_i F_3 * g_i F_3](\mathbf{r})$ and $[h_i F_3](\mathbf{r})$. We set this range to be $\mathcal{I}_{\text{skew}} = [k_{\text{min}}^{\tilde{P}}, k_{\text{max}}^{\tilde{P}}] = [0.035, 0.075] h\text{Mpc}^{-1}$ with bin-width $\Delta k^{\tilde{P}}$ chosen to be $0.01 h\text{Mpc}^{-1}$. Note that these choices ensure $\mathcal{I}_{\text{skew}} \subset \mathcal{I}_{\text{conv}}$ in order to discard modes on the boundary of $\mathcal{I}_{\text{conv}}$, which suffer larger numerical errors from the convolution.

For both power spectrum multipoles and skew-spectra, we subtract the expected Poisson shot-noise terms in order to minimize the potentially different noise features between the data and the simulations. The shot-noise of the power spectrum multipoles is given by: $\hat{P}^{\text{shot}}(k) = (1 + \alpha)I_{21}/I_{22}$. For the skew-spectra, we adopt the shot-noise contribution for the bispectrum [27], and follow Ref. [24] to adapt it for the skew-spectra:

$$\hat{P}_S^{\text{shot}}(k) = \sum_i \int \frac{d\hat{\mathbf{k}}}{4\pi} h_i(-\mathbf{k}) \left[\left(\frac{I_{31}}{I_{33}} + \frac{I_{32}\hat{P}(\mathbf{k})}{I_{33}} \right) [f_i * g_i](\mathbf{k}) + \frac{2I_{32}}{I_{33}} [\hat{P} f_i * g_i](\mathbf{k}) \right]. \quad (3.6)$$

where $\hat{P}(\mathbf{k})$ is the power spectrum estimated from data. Note that $I_{\lambda_1\lambda_2}$ here is the same as the one in Eq. (3.3). Despite these subtractions, we maintain nuisance parameters in our theory model, which measure the deviation from the Poisson prediction, and so the priors for nuisance parameters of the shot-noise will therefore be centered at zero shot-noise.

We use the code `nbodykit`¹¹ [67] to paint the catalogues onto a grid, as well as to facilitate our estimation of these spectra. In particular, we use the functions `ConvolvedFFTPower()` to estimate the power spectrum multipoles and `FFTPower()` to compute the skew-spectra (specifically, in the cross-correlation between the quadratic field and the linear field).

4 Parameter Inference

In this section, we will discuss details of our parameter inference and describe the choices we have made. We start with a discussion of our likelihood function and the covariance matrix, followed by a discussion of our sampling method and prior choices.

4.1 Likelihood Function

Working with the assumption of a Gaussian likelihood, we compute the covariance \hat{C} from 2048 Patchy mocks.

Our complete data vector is $\mathbf{d}^i = \{P_0^i, P_2^i, P_4^i, \tilde{P}_0^i, \tilde{P}_1^i, \tilde{P}_2^i, \tilde{P}_{\text{equil}}^i, \tilde{P}_{\text{ortho}}^i\}$, i.e. the power spectrum multipoles and skew-spectra with multiple shapes (where i here denotes the index for the simulation). In order to compute the covariance matrix, we first compute the quantity \hat{C}^* :

$$\hat{C}^* = \frac{1}{n-1} \sum_{i=1}^n (\mathbf{d}^i - \bar{\mathbf{d}})(\mathbf{d}^i - \bar{\mathbf{d}})^\top, \quad (4.1)$$

where $n = 2048$ is the number of simulations and $\bar{\mathbf{d}}$ is the sample mean of the data vector. We further include the Hartlap factor to make it an unbiased estimate of the covariance [68],

$$\hat{C} = \frac{n-1}{n-p-2} \hat{C}^*, \quad (4.2)$$

where p denotes the number of data points, or simply the length of the data vector \mathbf{d}^i .

As we assume a Gaussian likelihood, we perform the matrix inversion for the covariance matrix as follows. First, we separate the covariance matrix into a diagonal and an off-diagonal part: $\hat{C} = \hat{C}^{\text{diag}} + \hat{C}^{\text{offdiag}}$. The piece \hat{C}^{diag} is block diagonal, i.e. it contains the diagonal part of the covariance between all pairs of \hat{P}_ℓ and \hat{P}_{S_i} , while the off-diagonal part \hat{C}^{offdiag} contains all of the cross-correlation across different k -bins.

Next, we apply Singular Value Decomposition (SVD)¹² to the non-diagonal part: $\hat{C}^{\text{offdiag}} = USV$, where S is a square diagonal matrix and both U and V are unitary matrices. Using

¹¹<https://nbodykit.readthedocs.io/en/latest/>.

¹²SVD is a general decomposition wherein a matrix M may be written as a product USV , in terms of unitary matrices U and V and a rectangular diagonal matrix S .

the Woodbury formula¹³, the inverse of the covariance matrix can be written down as [69]:

$$\hat{\mathbf{C}}^{-1} = (\hat{\mathbf{C}}^{\text{diag}})^{-1} - (\hat{\mathbf{C}}^{\text{diag}})^{-1}US \left(I + V(\hat{\mathbf{C}}^{\text{diag}})^{-1}US \right)^{-1} V(\hat{\mathbf{C}}^{\text{diag}})^{-1}. \quad (4.3)$$

As a result, the inverse of the covariance now turns out to be a correction to the inverse of the diagonal matrix. Additionally, we note that the matrix $\hat{\mathbf{C}}^{\text{offdiag}}$ is of low rank, and the Woodbury formula enables us to perform the low-rank approximation of the inverse¹⁴. This procedure can help us reduce small numerical fluctuations in the inverse as well as speed-up the matrix product in the likelihood function.

With the Woodbury simplified covariance, the negative log-likelihood function can be broken down into diagonal and off-diagonal pieces:

$$-2 \log \mathcal{L} = -2 \log \mathcal{L}_{\text{diag}} - 2 \log \mathcal{L}_{\text{offdiag}}. \quad (4.4)$$

Here, $\mathcal{L}_{\text{diag}}$ and $\mathcal{L}_{\text{offdiag}}$ correspond to:

$$\begin{aligned} -2 \log \mathcal{L}_{\text{diag}} &= (\mathbf{d} - \mathbf{m})^\top (\hat{\mathbf{C}}^{\text{diag}})^{-1} (\mathbf{d} - \mathbf{m}), \\ -2 \log \mathcal{L}_{\text{offdiag}} &= - \left[U^\top (\hat{\mathbf{C}}^{\text{diag}})^{-1} (\mathbf{d} - \mathbf{m}) \right]^\top S \left(I + V(\hat{\mathbf{C}}^{\text{diag}})^{-1}US \right)^{-1} \left[V(\hat{\mathbf{C}}^{\text{diag}})^{-1} (\mathbf{d} - \mathbf{m}) \right], \end{aligned} \quad (4.5)$$

where \mathbf{d} is the data vector being either BOSS data or `Nseries` mocks, and \mathbf{m} is the vector containing the theoretically computed power spectrum multipoles and skew-spectra.

4.2 Parameters and Prior Choices

In our analysis, we assume a Λ CDM cosmology with parameters fixed to *Planck* 2018 best-fit values [70] and we set the sum of neutrino mass to be 60 meV. As a result, in addition to $f_{\text{NL}}^{\text{equil}}$ and $f_{\text{NL}}^{\text{ortho}}$, we vary the EFT parameters, i.e. the galaxy bias and the counterterms, as well as nuisance parameters for shot-noise in our analysis. We follow Refs. [10, 71, 72] for the choices of priors, which are motivated by previous BOSS analyses for the counterterms¹⁵ and by the co-evolution model [73] for the bias parameters. The priors for bias parameters are set up to be:

$$\begin{aligned} b_1 &\sim \text{Uniform}(0, 4), \quad b_2 \sim \text{Uniform}(-4, 4), \quad b_{\mathcal{G}_2} \sim \text{Uniform}(-4, 4), \\ b_{\Gamma_3} &\sim \mathcal{N}\left(\frac{23}{42}(b_1 - 1), 1^2\right), \end{aligned} \quad (4.6)$$

where $\mathcal{N}(\mu, \sigma^2)$ is a normal distribution with mean μ and variance σ^2 , and $\text{Uniform}(a, b)$ sets a flat prior between the bounds a and b .

¹³ $(A + UCV)^{-1} = A^{-1} - A^{-1}UC(I + VA^{-1}UC)^{-1}VA^{-1}$

¹⁴The idea of low-rank approximation is that we can get rid of small eigenvalues in S inside the SVD decomposition. That is, we set $S_{ii} = 0$ if $\max_{i'} S_{i'i'}/S_{ii} > c_{\text{LR}}$ for some threshold c_{LR} of our choice.

¹⁵The counterterms at one loop ($c_{0,2,4}$ and $c_{0,1,2}^{\text{B}}$) are expected to be $\mathcal{O}(1) \times k_{\text{NL}}^{-2}$. However, due to the strong FoG effect already detected in the BOSS sample we expect it to take a larger value than the naive EFT estimate, and the priors are taken to be wide enough to accommodate for this. Meanwhile, although \tilde{c} (in Eq. (2.21)) is at two-loop, previous power spectrum analyses detect a value much larger (~ 500 [Mpc/h]⁴) than the EFT estimate, and the prior is taken accordingly [42].

For the counterterms and the shot-noise parameters, we have:

$$\begin{aligned}
\frac{c_0}{[\text{Mpc}/h]^2} &\sim \mathcal{N}(0, 30^2), & \frac{c_2}{[\text{Mpc}/h]^2} &\sim \mathcal{N}(30, 30^2), & \frac{c_4}{[\text{Mpc}/h]^2} &\sim \mathcal{N}(0, 30^2), \\
\frac{\tilde{c}}{[\text{Mpc}/h]^4} &\sim \mathcal{N}(500, 500^2), & \frac{c_1^{\text{B}}}{[\text{Mpc}/h]^2} &\sim \mathcal{N}(0, 50^2), & \frac{c_0^{\text{B}}}{[\text{Mpc}/h]^2} &\sim \mathcal{N}(0, 50^2), \\
\frac{c_2^{\text{B}}}{[\text{Mpc}/h]^2} &\sim \mathcal{N}(0, 50^2), & A_{\text{shot}} &\sim \mathcal{N}(-1, 1^2), & P_{\text{shot}} &\sim \mathcal{N}(-1, 2^2), \\
B_{\text{shot}} &\sim \mathcal{N}(0, 1^2), & a_0 &\sim \mathcal{N}(0, 2^2), & a_2 &\sim \mathcal{N}(0, 2^2).
\end{aligned} \tag{4.7}$$

The counterterms $\{c_0, c_2, c_4\}$ here are related to $\{\tilde{c}_0, \tilde{c}_2, \tilde{c}_4\}$ (defined in §2) by the mapping [42]: $c_0 \equiv \tilde{c}_0 + f\tilde{c}_2/3 + f^2\tilde{c}_4/5$, $c_2 \equiv \frac{3}{4}(\tilde{c}_2 + 6f\tilde{c}_4/7)$ and $c_4 \equiv \frac{8}{35}\tilde{c}_4$ ¹⁶. We also note here that we include two additional parameters c_0^{B} and c_2^{B} for the skew-spectra (compared with a single counterterm as in Refs. [10, 71]), since our skew-spectra are sensitive to RSD information. For the primordial non-Gaussianity parameters, $f_{\text{NL}}^{\text{equil}}$ and $f_{\text{NL}}^{\text{ortho}}$, we adopt uninformative flat priors. In practice, we have

$$f_{\text{NL}}^{\text{equil}} \sim \text{Uniform}(-2000, 2000), \quad f_{\text{NL}}^{\text{ortho}} \sim \text{Uniform}(-1000, 1000). \tag{4.8}$$

For the non-local scale-dependent bias b_ζ , we have [10]:

$$b_\zeta = \bar{b}_\zeta \frac{18}{5} \delta_c (b_1 - 1) \text{ with } \bar{b}_\zeta \sim \mathcal{N}(1, 5) \text{ and } \delta_c = 1.686. \tag{4.9}$$

To sum up, we have a total of 17 nuisance parameters in each patch of the sky, so the total number of parameters are $17 \times N_{\text{patch}} + 2$, with N_{patch} being the number of patches. Since we use both CMASS and LOWZ redshift cuts, each with NGC and SGC skies, we have $N_{\text{patch}} = 4$, giving us a total of 70 parameters.

Finally, in order to sample our posterior, we will use nested sampling [74], which will be done with the public package `PolyChord`¹⁷ [75, 76].

5 Results and Discussions

Before analyzing the data, we first apply our pipeline to the `Nseries` mocks as a validation test, where our goal is to detect any potential statistical bias arising from our theoretical modelling. In other words, we seek to estimate the theoretical error intrinsic to our modelling choices. For this validation test, we use the mean of the power spectrum multipoles and skew-spectra across the 84 `Nseries` simulations as our data. We compute our covariance matrix using 2048 `Pathy` simulations, the same as the one used for BOSS CMASS NGC.

We perform two separate analyses using the `Nseries` data. One is to match the effective survey volume of BOSS DR12 ($V_{\text{eff}} = 6 h^{-3} \text{Gpc}^3$), which we approximate by rescaling the `Pathy` covariance matrix by a factor of 2.4. The other one is to match the total volume of the

¹⁶This mapping accounts for the change of basis of the counterterm parameters as one computes the multipoles of $P_{gg,\text{ctr}}(k, \mu)$ (see Eq (2.21)). In other words, it specifies the combination of the \tilde{c}_ℓ coefficients appearing in the power spectrum multipoles $P_{gg,\ell}(k)$. For example, $P_{gg,0}^{\text{ctr}}(k) = (\tilde{c}_0 + f\tilde{c}_2/3 + f^2\tilde{c}_4/5)k^2 P_L(k) \equiv c_0 k^2 P_L(k)$.

¹⁷<https://github.com/PolyChord/PolyChordLite>.

Nseries suite ($V_{\text{eff}} = 235 h^{-3} \text{Gpc}^3$), this time rescaling the covariance by 84. The two cases serve different purposes. We will use the full **Nseries** volume to estimate potential statistical biases, while using the other one to assess whether it will be significant under the noise level of BOSS DR12. In addition to the f_{NL} parameters, we vary the biases and counterterms in both analyses. Note that the **Nseries** simulations are only semi-independent, so our estimates for the theoretical error are expected to be conservative.

The result for each effective volume is presented in Table 2. For each volume, we show constraints for $f_{\text{NL}}^{\text{equil}}$ and $f_{\text{NL}}^{\text{ortho}}$ under three different cases: (1) varying only $f_{\text{NL}}^{\text{equil}}$, (2) varying only $f_{\text{NL}}^{\text{ortho}}$, and (3) varying both $f_{\text{NL}}^{\text{equil}}$ and $f_{\text{NL}}^{\text{ortho}}$. Varying only $f_{\text{NL}}^{\text{equil}}$ we find that the bias on the equilateral shape is around 0.53σ away from zero when compared with the BOSS level error. However for the orthogonal shape, the theoretical error is at the 4.15σ level, indicating a significant bias due to our treatment of the survey geometry. Even though in Appendix B we observed that our approximate window convolution leads to an 18% error on the skew-spectra sourced by the orthogonal shape, it is sufficient to cause a severe systematic bias in the full analysis. We arrive at the same conclusion upon jointly varying $f_{\text{NL}}^{\text{equil}}$ and $f_{\text{NL}}^{\text{ortho}}$, finding a significant bias for the latter. As a consequence, in our final analysis on BOSS DR12, we will only vary $f_{\text{NL}}^{\text{equil}}$.

We additionally inspect each skew-spectrum shape to isolate the source of these errors. To be precise, we perform the same **Nseries** validation test as above while restricting the skew-spectra to a single shape \tilde{P}_i in our data vector. In doing so we find that restricting the data to just \tilde{P}_0 leads to a theoretical error on $f_{\text{NL}}^{\text{ortho}}$ within 0.4σ , relative to BOSS errors. However, the other kernels are more error prone, maintaining a theoretical error of $1 - 2\sigma$. Our results can be compared with those of Ref. [12], where the same approximate window convolution is used, albeit on the one-loop bispectrum monopole. They find a negligible theoretical error on $f_{\text{NL}}^{\text{ortho}}$, which is consistent with our checks, since \tilde{P}_0 is nothing more than an average of the bispectrum monopole. These tests suggest that the window-approximation could be used in order to estimate $f_{\text{NL}}^{\text{ortho}}$ using the bispectrum monopole data, but may be too imprecise for the other bispectrum multipoles, at the level of BOSS sensitivity.

Effective Volume (Nseries)	$V_{\text{eff}} = 6 h^{-3} \text{Gpc}^3$		$V_{\text{eff}} = 235 h^{-3} \text{Gpc}^3$	
	$f_{\text{NL}}^{\text{equil}}$	$f_{\text{NL}}^{\text{ortho}}$	$f_{\text{NL}}^{\text{equil}}$	$f_{\text{NL}}^{\text{ortho}}$
$f_{\text{NL}}^{\text{equil}}$ only	36 ± 758	—	404 ± 81	—
$f_{\text{NL}}^{\text{ortho}}$ only	—	69 ± 221	—	919 ± 24
$f_{\text{NL}}^{\text{equil}} + f_{\text{NL}}^{\text{ortho}}$	241 ± 778	56 ± 204	194 ± 88	827 ± 20

Table 2. Posterior means and variances of $f_{\text{NL}}^{\text{equil}}$ and $f_{\text{NL}}^{\text{ortho}}$ with **Nseries** mocks. We consider two different effective volumes, $6 h^{-3} \text{Gpc}^3$ and $235 h^{-3} \text{Gpc}^3$, which allows us to determine the size of the systematic errors compared with the noise level of BOSS DR12.

Having validated our pipeline and detected any potential bias, we present our main constraint for primordial non-Gaussianity $f_{\text{NL}}^{\text{equil}}$ utilizing the full BOSS DR12 dataset:

$$f_{\text{NL}}^{\text{equil}} \text{ varied only: } f_{\text{NL}}^{\text{equil}} = -34_{-34}^{+296} \text{ at } 68\% \text{ CL}, \quad (5.1)$$

with the contour plot shown in Figure 1. Our result indicates that $f_{\text{NL}}^{\text{equil}}$ is consistent with zero at 68% CL even if we include a potential 0.54σ statistical bias from our `Nseries` analysis. This result is also consistent within 1σ with Refs. [10, 12], which find $f_{\text{NL}}^{\text{equil}} = 260 \pm 300$ and $f_{\text{NL}}^{\text{equil}} = 245 \pm 293$, respectively. As some of the priors on the EFT parameters are poorly known beforehand, we have also checked that widening them by $5\times$ leads to similar constraints for the $f_{\text{NL}}^{\text{equil}}$ parameter.

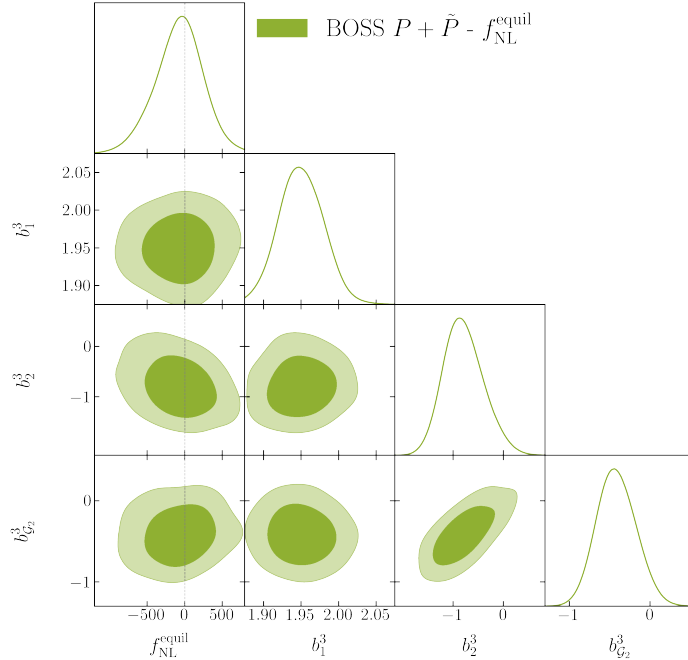


Figure 1. Posterior distributions for our full BOSS analysis, where we vary only $f_{\text{NL}}^{\text{equil}}$ and all the EFT parameters. The bias parameters shown here are for CMASS NGC only, indicated by the index 3. We fix the Λ CDM cosmological parameters to *Planck* 2018 best-fit values. The expected Poisson shot-noise contribution is subtracted from the BOSS data.

Let us now compare the results of our main analysis to the ones in the literature. We start with the constraints reported in Ref. [12], which uses the power spectrum monopole and quadrupole, and the bispectrum monopole, all at the one-loop level. As in our work, Ref. [12] uses the FKP formalism and fixes the Λ CDM parameters to *Planck* 2018 values. However, we use a different set of priors for the EFT parameters. Our choice follows Refs. [10, 71, 72] (discussed in §4), which employs Gaussian priors with larger variances compared to Ref. [12]. In addition, instead of a lognormal prior on b_1 centered at $e^{0.8}$ and Gaussian priors on both b_2 and $b_{\mathcal{G}_2}$ centered at zero, we impose uniform priors for all of them. Overall, we have a comparable variance, i.e. a 7.5% difference between our $\sigma(f_{\text{NL}}^{\text{equil}})$ and the one of Ref. [12] despite our usage of only the tree-level bispectrum.

We also compare our result with another recent work [10], which analyzes the window-less power spectrum multipoles and the bispectrum monopole [77, 78]. In particular, we will focus on the comparison with the aggressive model in Ref. [10]. This model fixes the Λ CDM parameters to *Planck* 2018 values. A co-evolution model is also assumed to fix the value of

the quadratic biases b_2 and b_{G_2} as a function of b_1 . Following this strategy, we also see a comparable level of error on $f_{\text{NL}}^{\text{equil}}$, i.e. within 5% differences on $\sigma(f_{\text{NL}}^{\text{equil}})$, between our result and theirs. Overall, our estimation of $f_{\text{NL}}^{\text{equil}}$ is consistent with theirs within 1σ .

With these comparisons, we can see that even though the skew-spectrum serves as a compression of the full bispectrum, the error bars we present are competitive with the full bispectrum analysis. This was also noted in our previous work [26] with harmonic-space skew-spectra in which we have shown, through a Fisher forecast, that skew-spectra with Legendre polynomial kernels are sufficient to constrain not only the bias parameters, but also the seven $\nu\Lambda\text{CDM}$ parameters. In this work, we include two additional kernels to capture shapes from primordial non-Gaussianity. We see that the addition of these two kernels reduces our error bars on $f_{\text{NL}}^{\text{equil}}$ and the EFT parameters by 10% – 20%, compared to the case with just Legendre polynomial kernels.

Finally, we point out some possible sources of systematic errors in our analysis. While our `Nseries` tests reveal an unimportant level of theoretical error on $f_{\text{NL}}^{\text{equil}}$, our posterior mean is still shifted away from zero. Part of these shifts come from our approximate treatment of the window convolution. As mentioned in §2, this approximation induces up to 5% errors on the gravitational contribution to the bispectrum, for scales larger than $k = 0.03 h\text{Mpc}^{-1}$. In Appendix B we also assess the impact of this approximation on both equilateral and orthogonal shapes, where we found a 6% error for the equilateral shape and 18% error for the orthogonal shape. This error compounds into a large theoretical error for $f_{\text{NL}}^{\text{ortho}}$, as we have seen from the `Nseries` validation tests. Another source of error may be the difference in shot-noise between the `Patchy` and `Nseries` simulations. We tested this by running our pipeline without subtracting the shot-noise from the data and found that our posterior shifts further away by 0.59σ for $f_{\text{NL}}^{\text{equil}}$, implying that different noise features between the mocks and the data may be a contributing factor. However, we note that the shift from the fiducial f_{NL} values remains below 1σ . Finally, in our validation test, we have used the `Patchy` mocks in order to approximate the covariance for the `Nseries` suite. This may further be a source of error since the two simulations have slightly different masks.

6 Conclusions

In this work we present the first analysis of BOSS DR12 galaxy-clustering data using weighted skew-spectra, jointly with the power spectrum multipoles, to probe primordial non-Gaussianity sourced by single-field inflation. Even though the skew-spectra serve the role of a dimension reduction of the full bispectrum, they have been shown to preserve almost all the information for not only amplitude-like parameters, but also $\nu\Lambda\text{CDM}$ parameters [22, 24, 26]. Here we constrain $f_{\text{NL}}^{\text{equil}}$, finding consistency with Refs. [10] and [12], which use the combination of the galaxy power spectrum multipoles and the bispectrum monopole.

Motivated by our previous work in harmonic space [26], which shows that the Legendre polynomial kernels for skew-spectra are sufficient to capture most of the information from the full bispectrum, we construct our skew-spectra with five different kernels, including Legendre polynomials, and two additional kernels based on the equilateral and orthogonal primordial

bispectrum templates. Each of them can extract non-degenerate information from the galaxy bispectrum.

Starting from the galaxy catalogue, we apply the FKP formalism to compute both power spectrum multipoles and skew-spectra. To model both of these statistics, we follow the effective field theory of large-scale structure approach, which requires several nuisance parameters such as galaxy biases, counterterms and shot-noise parameters. The survey geometry is also taken into account by convolving the targeted spectra with appropriate window functions. In particular we rely on an approximate treatment of the survey geometry for the skew-spectra.

We assume a Gaussian likelihood and construct our covariance matrix with 2048 `Patchy` mocks. Due to the large number of parameters in our theory model, we use the nested sampling algorithm to estimate the posterior distributions for both $f_{\text{NL}}^{\text{equil}}$ and $f_{\text{NL}}^{\text{ortho}}$, marginalizing over the EFT parameters. We first test our pipeline on `Nseries` mocks and obtain a theoretical error on $f_{\text{NL}}^{\text{equil}}$ to within 1σ , relative to BOSS level error. However, we find that the window approximation on the primordial bispectrum causes a significant bias on $f_{\text{NL}}^{\text{ortho}}$. Therefore in our final analysis on BOSS DR12 data we choose to only constrain $f_{\text{NL}}^{\text{equil}}$. Fixing the cosmology to *Planck* 2018 best-fit values, we obtain $f_{\text{NL}}^{\text{equil}} = -34_{-33}^{+296}$ at 68% CL, consistent with zero. We find no evidence for primordial non-Gaussianity, which is consistent with the findings of Refs. [12] and [10].

This work is a first step in applying the skew-spectra to galaxy survey data. There are some directions in which we plan to make further progress. First, we use an approximate treatment of the window convolution on the bispectrum, which prevents us from reliably estimating $f_{\text{NL}}^{\text{ortho}}$. Moreover, even for the other bispectrum shapes, this approximation restricts the number of large-scale modes accessible to us. Since primordial signals exist in both large-scale and small-scale fluctuations, circumventing this issue would provide a clear path to improving our constraining power. Secondly, we perform a high-dimensional numerical integral in order to obtain our theory skew-spectra, which is a time-consuming task and therefore prevents us from varying the full $\nu\Lambda\text{CDM}$ parameters simultaneously in the likelihood analysis. This could be potentially accomplished with help of simulation-based inference methods [79–83]. Lastly, we note that our analysis has used an approximation to determine the normalization of the bispectrum (I_{33} mentioned in §3.1), similar to the approximation for I_{22} made at the power spectrum level. This could be a source of systematic error for f_{NL} (similar to the error on σ_8 caused by approximating I_{22}). While our validation tests verify that this error is small for BOSS data, one should rigorously check this for upcoming surveys.

Acknowledgments

We thank Guido D’Amico, Misha Ivanov, Oliver Philcox, and Georgios Valogiannis for insightful discussions. CD and SFC are partially supported by the Department of Energy (DOE) Grant No. DE-SC0020223. PC is supported by the DOE Grant No. DE-SC0013607. We acknowledge the use of `CAMB`¹⁸ [84] and `CLASS-PT` [42] (an extension of `CLASS` [43]) for theoretical computation; `pycuba` [53, 54] for numerical integration; `nbodykit` [67] and

¹⁸<https://camb.info>

`Corrfunc` [63] for analysis of simulations and data; `PolyChord` [75, 76] for parameter inference, and `GetDist`¹⁹ [85] to generate posterior distributions.

¹⁹<https://getdist.readthedocs.io/en/latest>

A BAO Damping

The damping of the BAO feature at low redshifts can be captured by performing an infrared resummation on the so-called wiggly part of the matter power spectrum [41]. For this, we first need to split the wiggly and non-wiggly parts of the matter power spectrum. Instead of using the standard Hu-Eisenstein fitting formula [86] for the smooth part of the power spectrum, we isolate the BAO feature, following Refs. [42, 87]. This procedure uses the Discrete Fast Sine transformation (DST) to identify the BAO bump in the real-space correlation function, and thus separate it to obtain the so-called wiggly part of the power spectrum.

Once we get the wiggly (P_w) and non-wiggly (P_{nw}) parts of the matter power spectrum, we can obtain the infrared resummed power spectrum:

$$P_{L,IR}(k) = P_{nw}(k) + e^{-k^2 \Sigma_{tot}^2} P_w(k). \quad (\text{A.1})$$

Here Σ_{tot}^2 is defined as [41, 88]:

$$\begin{aligned} \Sigma^2 &= \frac{1}{6\pi^2} \int_0^\Lambda dq P_{nw}(q) [1 - j_0(qx_{osc}) + 2j_2(qx_{osc})], \\ \Sigma_{tot}^2 &= -\frac{2}{15} f^2 \delta \Sigma^2 + \left(1 + \frac{1}{3} f(2+f)\right) \Sigma^2, \\ \delta \Sigma^2 &= \frac{1}{2\pi^2} \int_0^\Lambda dq P_{nw}(q) j_2(qx_{osc}), \end{aligned} \quad (\text{A.2})$$

and we set $\Lambda = 0.1 \text{ hMpc}^{-1}$ and $x_{osc} = 110 \text{ h}^{-1}\text{Mpc}$.

B Survey Geometry Approximation

As mentioned in §2.4, we approximate the impact of the survey geometry in our theoretical skew-spectra computation following Refs. [27, 49] where we only convolve factors of the power spectrum with the window function. Since we are working with non-Gaussian initial conditions, our bispectrum, and therefore skew-spectra, contain both contributions due to gravitational nonlinearities and also due to the primordial bispectrum. References [27, 49] only assess this approximation on the gravitational terms, finding at most an error of 5%. In this appendix, we will quantify the error on our skew-spectra due to this approximation, specifically targeting the primordial contribution.

As a first step, we estimate the exact window convolved skew-spectra. To do so we will generate a large number of synthetic non-Gaussian density fields, appropriately masked. From each of these we may estimate our desired skew-spectrum, ultimately averaging over all of our mocks. To generate our boxes we use the same survey specification as the CMASS NGC patch (see §3).

In order to generate our synthetic density field, we start with a Gaussian random field ϕ generated using the primordial power spectrum $P_\phi(k) = A_s k^{-3}$ ²⁰. Next, we generate a

²⁰For the purpose of this test we set $n_s = 1$ in order to simplify the analysis. We do not expect this choice to significantly impact our conclusions.

non-Gaussian field Φ for both equilateral and orthogonal configurations from this Gaussian random field ϕ as [89, 90]:

$$\Phi_{\text{equil}} = \phi + f_{\text{NL}} [-3\phi^2 + 4\partial^{-1}(\phi\partial\phi) + 2\nabla^{-2}(\phi\nabla^2\phi) - 2\nabla^{-2}(\partial\phi)^2] \quad (\text{B.1})$$

$$\begin{aligned} \Phi_{\text{ortho}} = \phi + 3f_{\text{NL}} & \left[-\left(1 + \frac{9p}{27}\right)\phi^2 - \left(2 + \frac{60p}{27}\right)\frac{1}{3}\nabla^{-2}(\partial\phi)^2 \right. \\ & + 2\left(1 + \frac{15p}{27}\right) \left((1-t)\partial^{-1}(\phi\partial\phi) + t\nabla^{-2}(\phi\nabla^2\phi) \right) \\ & \left. + \frac{p}{27}\nabla^2(\partial^{-1}\phi\partial^{-1}\phi) - \frac{20p}{27}\partial^{-1}(\nabla^2\phi\partial^{-1}\phi) - \frac{12p}{27}\partial(\phi\partial^{-1}\phi) + \frac{30p}{27}\partial\phi\partial^{-1}\phi \right], \quad (\text{B.2}) \end{aligned}$$

where $t = \frac{2+60p/27}{6(1+15p/27)}$ and $p = 8.52587$. Note that Φ_{equil} will have a nontrivial bispectrum equal to the equilateral shape, and likewise for Φ_{ortho} . These parametrizations also ensure that the largest correction to the power spectrum scales as k^{-2} . We subsequently evolve this primordial density field into a late-time matter density field by multiplying by the matter transfer function $T(k, z)$. In order to simulate a galaxy overdensity field, we include a factor of $b_1 + f\mu^2$ to simulate the galaxy bias b_1 and redshift-space distortion. To account for the survey geometry, we directly apply the meshed FKP weight $1/(1 + \bar{n}_g(z)P_{\text{FKP}})$ on each pixel in our simulation box.

With this pipeline for generating the non-Gaussian field, we simulate 10,000 such maps for both equilateral and orthogonal PNG. Note that by construction, these synthetic fields only contain non-Gaussian information due to the primordial contribution. This enables us to isolate the contribution to each of the skew-spectra sourced by PNG. We then average over skew-spectra estimated from each of these boxes in order to obtain an estimate of the exact window convolved skew-spectra.

In Table 3 we list the percentage difference between the exact window convolved skew-spectra and those computed using the approximation specified in §2.4. Note that in quoting these numbers, we discard k modes for which the skew-spectra almost vanish, since these modes are noisier and in any case contain too little power to impact f_{NL} constraints. We see that for equilateral PNG, the fractional errors are well within at most 6.3% except for \tilde{P}_{ortho} . However, this is not problematic since this shape has limited sensitivity to $f_{\text{NL}}^{\text{equil}}$. On the other hand, for orthogonal PNG, the fractional errors are in general larger, ranging from 9.2% to 18.3%.

Skew-spectrum	\tilde{P}_0	\tilde{P}_1	\tilde{P}_2	\tilde{P}_{equil}	\tilde{P}_{ortho}
Equilateral PNG	4.6%	6.3%	5.3%	3.6%	15.4%
Orthogonal PNG	18.3%	10.0%	14.8%	17.8%	9.2%

Table 3. Fractional error between the exact window convolved skew-spectra (obtained from the average over simulations) and the approximate theoretical computation. We consider both equilateral and orthogonal configurations, and for each skew-spectrum we show the maximum percent error across all k modes.

References

- [1] N. Bartolo, E. Komatsu, S. Matarrese, and A. Riotto, “Non-Gaussianity from inflation: Theory and observations,” *Phys. Rept.* **402** (2004) 103–266, [arXiv:astro-ph/0406398](#).
- [2] E. Komatsu *et al.*, “Non-Gaussianity as a Probe of the Physics of the Primordial Universe and the Astrophysics of the Low Redshift Universe,” [arXiv:0902.4759](#) [[astro-ph.CO](#)].
- [3] P. D. Meerburg *et al.*, “Primordial Non-Gaussianity,” [arXiv:1903.04409](#) [[astro-ph.CO](#)].
- [4] A. Achúcarro *et al.*, “Inflation: Theory and Observations,” [arXiv:2203.08128](#) [[astro-ph.CO](#)].
- [5] C. Cheung, P. Creminelli, A. L. Fitzpatrick, J. Kaplan, and L. Senatore, “The Effective Field Theory of Inflation,” *JHEP* **03** (2008) 014, [arXiv:0709.0293](#) [[hep-th](#)].
- [6] **Planck** Collaboration, Y. Akrami *et al.*, “Planck 2018 results. IX. Constraints on primordial non-Gaussianity,” *Astron. Astrophys.* **641** (2020) A9, [arXiv:1905.05697](#) [[astro-ph.CO](#)].
- [7] V. Desjacques and U. Seljak, “Primordial non-Gaussianity from the large scale structure,” *Class. Quant. Grav.* **27** (2010) 124011, [arXiv:1003.5020](#) [[astro-ph.CO](#)].
- [8] **BOSS** Collaboration, K. S. Dawson *et al.*, “The Baryon Oscillation Spectroscopic Survey of SDSS-III,” *Astron. J.* **145** (2013) 10, [arXiv:1208.0022](#) [[astro-ph.CO](#)].
- [9] **BOSS** Collaboration, S. Alam *et al.*, “The clustering of galaxies in the completed SDSS-III Baryon Oscillation Spectroscopic Survey: cosmological analysis of the DR12 galaxy sample,” *Mon. Not. Roy. Astron. Soc.* **470** no. 3, (2017) 2617–2652, [arXiv:1607.03155](#) [[astro-ph.CO](#)].
- [10] G. Cabass, M. M. Ivanov, O. H. E. Philcox, M. Simonović, and M. Zaldarriaga, “Constraints on Single-Field Inflation from the BOSS Galaxy Survey,” *Phys. Rev. Lett.* **129** no. 2, (2022) 021301, [arXiv:2201.07238](#) [[astro-ph.CO](#)].
- [11] G. Cabass, M. M. Ivanov, O. H. E. Philcox, M. Simonović, and M. Zaldarriaga, “Constraints on multifield inflation from the BOSS galaxy survey,” *Phys. Rev. D* **106** no. 4, (2022) 043506, [arXiv:2204.01781](#) [[astro-ph.CO](#)].
- [12] G. D’Amico, M. Lewandowski, L. Senatore, and P. Zhang, “Limits on primordial non-Gaussianities from BOSS galaxy-clustering data,” [arXiv:2201.11518](#) [[astro-ph.CO](#)].
- [13] B. Leistedt, H. V. Peiris, and N. Roth, “Constraints on Primordial Non-Gaussianity from 800 000 Photometric Quasars,” *Phys. Rev. Lett.* **113** no. 22, (2014) 221301, [arXiv:1405.4315](#) [[astro-ph.CO](#)].
- [14] E. Castorina *et al.*, “Redshift-weighted constraints on primordial non-Gaussianity from the clustering of the eBOSS DR14 quasars in Fourier space,” *JCAP* **09** (2019) 010, [arXiv:1904.08859](#) [[astro-ph.CO](#)].
- [15] E.-M. Mueller *et al.*, “The clustering of galaxies in the completed SDSS-IV extended Baryon Oscillation Spectroscopic Survey: Primordial non-Gaussianity in Fourier Space,” [arXiv:2106.13725](#) [[astro-ph.CO](#)].
- [16] **DESI** Collaboration, A. Aghamousa *et al.*, “The DESI Experiment Part I: Science, Targeting, and Survey Design,” [arXiv:1611.00036](#) [[astro-ph.IM](#)].
- [17] LSST Science Collaboration, “LSST Science Book, Version 2.0,” *arXiv e-prints* (Dec., 2009) [arXiv:0912.0201](#), [arXiv:0912.0201](#) [[astro-ph.IM](#)].

- [18] O. Doré *et al.*, “Cosmology with the SPHEREX All-Sky Spectral Survey,” [arXiv:1412.4872 \[astro-ph.CO\]](#).
- [19] L. Amendola *et al.*, “Cosmology and fundamental physics with the Euclid satellite,” *Living Rev. Rel.* **21** no. 1, (2018) 2, [arXiv:1606.00180 \[astro-ph.CO\]](#).
- [20] M. Schmittfull, T. Baldauf, and U. Seljak, “Near optimal bispectrum estimators for large-scale structure,” *Phys. Rev. D* **91** no. 4, (2015) 043530, [arXiv:1411.6595 \[astro-ph.CO\]](#).
- [21] E. Komatsu, D. N. Spergel, and B. D. Wandelt, “Measuring primordial non-Gaussianity in the cosmic microwave background,” *Astrophys. J.* **634** (2005) 14–19, [arXiv:astro-ph/0305189](#).
- [22] A. Moradinezhad Dizgah, H. Lee, M. Schmittfull, and C. Dvorkin, “Capturing non-Gaussianity of the large-scale structure with weighted skew-spectra,” *JCAP* **04** (2020) 011, [arXiv:1911.05763 \[astro-ph.CO\]](#).
- [23] M. Schmittfull and A. Moradinezhad Dizgah, “Galaxy skew-spectra in redshift-space,” *JCAP* **03** (2021) 020, [arXiv:2010.14267 \[astro-ph.CO\]](#).
- [24] J. Hou, A. Moradinezhad Dizgah, C. Hahn, and E. Massara, “Cosmological Information in Skew Spectra of Biased Tracers in Redshift Space,” [arXiv:2210.12743 \[astro-ph.CO\]](#).
- [25] D. Munshi, T. Namikawa, T. D. Kitching, J. D. McEwen, and F. R. Bouchet, “Weak Lensing Skew-Spectrum,” *Mon. Not. Roy. Astron. Soc.* **498** no. 4, (2020) 6057–6068, [arXiv:2006.12832 \[astro-ph.CO\]](#).
- [26] P. Chakraborty, S.-F. Chen, and C. Dvorkin, “Skewing the CMB×LSS: a fast method for bispectrum analysis,” *JCAP* **07** no. 07, (2022) 038, [arXiv:2202.11724 \[astro-ph.CO\]](#).
- [27] H. Gil-Marín, J. Noreña, L. Verde, W. J. Percival, C. Wagner, M. Manera, and D. P. Schneider, “The power spectrum and bispectrum of SDSS DR11 BOSS galaxies – I. Bias and gravity,” *Mon. Not. Roy. Astron. Soc.* **451** no. 1, (2015) 539–580, [arXiv:1407.5668 \[astro-ph.CO\]](#).
- [28] J. R. Fergusson, D. M. Regan, and E. P. S. Shellard, “Rapid Separable Analysis of Higher Order Correlators in Large Scale Structure,” *Phys. Rev. D* **86** (2012) 063511, [arXiv:1008.1730 \[astro-ph.CO\]](#).
- [29] P. Creminelli, A. Nicolis, L. Senatore, M. Tegmark, and M. Zaldarriaga, “Limits on non-gaussianities from wmap data,” *JCAP* **05** (2006) 004, [arXiv:astro-ph/0509029](#).
- [30] D. Babich, P. Creminelli, and M. Zaldarriaga, “The Shape of non-Gaussianities,” *JCAP* **08** (2004) 009, [arXiv:astro-ph/0405356](#).
- [31] L. Senatore, K. M. Smith, and M. Zaldarriaga, “Non-Gaussianities in Single Field Inflation and their Optimal Limits from the WMAP 5-year Data,” *JCAP* **01** (2010) 028, [arXiv:0905.3746 \[astro-ph.CO\]](#).
- [32] **Planck** Collaboration, Y. Akrami *et al.*, “Planck 2018 results. X. Constraints on inflation,” *Astron. Astrophys.* **641** (2020) A10, [arXiv:1807.06211 \[astro-ph.CO\]](#).
- [33] J. J. M. Carrasco, M. P. Hertzberg, and L. Senatore, “The Effective Field Theory of Cosmological Large Scale Structures,” *JHEP* **09** (2012) 082, [arXiv:1206.2926 \[astro-ph.CO\]](#).
- [34] D. Baumann, A. Nicolis, L. Senatore, and M. Zaldarriaga, “Cosmological Non-Linearities as an Effective Fluid,” *JCAP* **07** (2012) 051, [arXiv:1004.2488 \[astro-ph.CO\]](#).
- [35] T. Nishimichi, G. D’Amico, M. M. Ivanov, L. Senatore, M. Simonović, M. Takada, M. Zaldarriaga, and P. Zhang, “Blinded challenge for precision cosmology with large-scale

- structure: results from effective field theory for the redshift-space galaxy power spectrum,” *Phys. Rev. D* **102** no. 12, (2020) 123541, [arXiv:2003.08277 \[astro-ph.CO\]](#).
- [36] M. M. Ivanov, O. H. E. Philcox, T. Nishimichi, M. Simonović, M. Takada, and M. Zaldarriaga, “Precision analysis of the redshift-space galaxy bispectrum,” *Phys. Rev. D* **105** no. 6, (2022) 063512, [arXiv:2110.10161 \[astro-ph.CO\]](#).
- [37] A. Perko, L. Senatore, E. Jennings, and R. H. Wechsler, “Biased Tracers in Redshift Space in the EFT of Large-Scale Structure,” [arXiv:1610.09321 \[astro-ph.CO\]](#).
- [38] L. Senatore and M. Zaldarriaga, “Redshift Space Distortions in the Effective Field Theory of Large Scale Structures,” [arXiv:1409.1225 \[astro-ph.CO\]](#).
- [39] L. Senatore and M. Zaldarriaga, “The IR-resummed Effective Field Theory of Large Scale Structures,” *JCAP* **02** (2015) 013, [arXiv:1404.5954 \[astro-ph.CO\]](#).
- [40] T. Baldauf, M. Mirbabayi, M. Simonović, and M. Zaldarriaga, “Equivalence Principle and the Baryon Acoustic Peak,” *Phys. Rev. D* **92** no. 4, (2015) 043514, [arXiv:1504.04366 \[astro-ph.CO\]](#).
- [41] M. M. Ivanov and S. Sibiryakov, “Infrared Resummation for Biased Tracers in Redshift Space,” *JCAP* **07** (2018) 053, [arXiv:1804.05080 \[astro-ph.CO\]](#).
- [42] A. Chudaykin, M. M. Ivanov, O. H. E. Philcox, and M. Simonović, “Nonlinear perturbation theory extension of the Boltzmann code CLASS,” *Phys. Rev. D* **102** no. 6, (2020) 063533, [arXiv:2004.10607 \[astro-ph.CO\]](#).
- [43] D. Blas, J. Lesgourgues, and T. Tram, “The Cosmic Linear Anisotropy Solving System (CLASS) II: Approximation schemes,” *JCAP* **07** (2011) 034, [arXiv:1104.2933 \[astro-ph.CO\]](#).
- [44] F. Bernardeau, S. Colombi, E. Gaztanaga, and R. Scoccimarro, “Large scale structure of the universe and cosmological perturbation theory,” *Phys. Rept.* **367** (2002) 1–248, [arXiv:astro-ph/0112551](#).
- [45] N. Dalal, O. Dore, D. Huterer, and A. Shirokov, “The imprints of primordial non-gaussianities on large-scale structure: scale dependent bias and abundance of virialized objects,” *Phys. Rev. D* **77** (2008) 123514, [arXiv:0710.4560 \[astro-ph\]](#).
- [46] V. Assassi, D. Baumann, and F. Schmidt, “Galaxy Bias and Primordial Non-Gaussianity,” *JCAP* **12** (2015) 043, [arXiv:1510.03723 \[astro-ph.CO\]](#).
- [47] **BOSS** Collaboration, F. Beutler *et al.*, “The clustering of galaxies in the completed SDSS-III Baryon Oscillation Spectroscopic Survey: baryon acoustic oscillations in the Fourier space,” *Mon. Not. Roy. Astron. Soc.* **464** no. 3, (2017) 3409–3430, [arXiv:1607.03149 \[astro-ph.CO\]](#).
- [48] C. Alcock and B. Paczynski, “An evolution free test for non-zero cosmological constant,” *Nature* **281** (1979) 358–359.
- [49] H. Gil-Marín, W. J. Percival, L. Verde, J. R. Brownstein, C.-H. Chuang, F.-S. Kitaura, S. A. Rodríguez-Torres, and M. D. Olmstead, “The clustering of galaxies in the SDSS-III Baryon Oscillation Spectroscopic Survey: RSD measurement from the power spectrum and bispectrum of the DR12 BOSS galaxies,” *Mon. Not. Roy. Astron. Soc.* **465** no. 2, (2017) 1757–1788, [arXiv:1606.00439 \[astro-ph.CO\]](#).
- [50] **BOSS** Collaboration, F. Beutler *et al.*, “The clustering of galaxies in the completed SDSS-III Baryon Oscillation Spectroscopic Survey: Anisotropic galaxy clustering in Fourier-space,” *Mon. Not. Roy. Astron. Soc.* **466** no. 2, (2017) 2242–2260, [arXiv:1607.03150 \[astro-ph.CO\]](#).

- [51] M. Karamanis and F. Beutler, “hankl: A lightweight Python implementation of the FFTLog algorithm for Cosmology,” [arXiv:2106.06331](#) [[astro-ph.IM](#)].
- [52] A. J. S. Hamilton, “Uncorrelated modes of the nonlinear power spectrum,” *Mon. Not. Roy. Astron. Soc.* **312** (2000) 257–284, [arXiv:astro-ph/9905191](#).
- [53] T. Hahn, “CUBA: A Library for multidimensional numerical integration,” *Comput. Phys. Commun.* **168** (2005) 78–95, [arXiv:hep-ph/0404043](#).
- [54] J. Buchner, A. Georgakakis, K. Nandra, L. Hsu, C. Rangel, M. Brightman, A. Merloni, M. Salvato, J. Donley, and D. Kocevski, “X-ray spectral modelling of the AGN obscuring region in the CDFS: Bayesian model selection and catalogue,” *Astron. Astrophys.* **564** (2014) A125, [arXiv:1402.0004](#) [[astro-ph.HE](#)].
- [55] SDSS-III Collaboration, S. Alam *et al.*, “The Eleventh and Twelfth Data Releases of the Sloan Digital Sky Survey: Final Data from SDSS-III,” *Astrophys. J. Suppl.* **219** no. 1, (2015) 12, [arXiv:1501.00963](#) [[astro-ph.IM](#)].
- [56] F.-S. Kitaura *et al.*, “The clustering of galaxies in the SDSS-III Baryon Oscillation Spectroscopic Survey: mock galaxy catalogues for the BOSS Final Data Release,” *Mon. Not. Roy. Astron. Soc.* **456** no. 4, (2016) 4156–4173, [arXiv:1509.06400](#) [[astro-ph.CO](#)].
- [57] S. A. Rodríguez-Torres *et al.*, “The clustering of galaxies in the SDSS-III Baryon Oscillation Spectroscopic Survey: modelling the clustering and halo occupation distribution of BOSS CMASS galaxies in the Final Data Release,” *Mon. Not. Roy. Astron. Soc.* **460** no. 2, (2016) 1173–1187, [arXiv:1509.06404](#) [[astro-ph.CO](#)].
- [58] C. Hahn, R. Scoccimarro, M. R. Blanton, J. L. Tinker, and S. A. Rodríguez-Torres, “The effect of fibre collisions on the galaxy power spectrum multipoles,” *Mon. Not. Roy. Astron. Soc.* **467** no. 2, (2017) 1940–1956, [arXiv:1609.01714](#) [[astro-ph.CO](#)].
- [59] M. E. C. Swanson, M. Tegmark, A. J. S. Hamilton, and J. C. Hill, “Methods for Rapidly Processing Angular Masks of Next-Generation Galaxy Surveys,” *Mon. Not. Roy. Astron. Soc.* **387** (2008) 1391, [arXiv:0711.4352](#) [[astro-ph](#)].
- [60] H. A. Feldman, N. Kaiser, and J. A. Peacock, “Power spectrum analysis of three-dimensional redshift surveys,” *Astrophys. J.* **426** (1994) 23–37, [arXiv:astro-ph/9304022](#).
- [61] F. Beutler and P. McDonald, “Unified galaxy power spectrum measurements from 6dFGS, BOSS, and eBOSS,” *JCAP* **11** (2021) 031, [arXiv:2106.06324](#) [[astro-ph.CO](#)].
- [62] A. de Mattia *et al.*, “The Completed SDSS-IV extended Baryon Oscillation Spectroscopic Survey: measurement of the BAO and growth rate of structure of the emission line galaxy sample from the anisotropic power spectrum between redshift 0.6 and 1.1,” *Mon. Not. Roy. Astron. Soc.* **501** no. 4, (2021) 5616–5645, [arXiv:2007.09008](#) [[astro-ph.CO](#)].
- [63] M. Sinha and L. H. Garrison, “corrfunc – a suite of blazing fast correlation functions on the CPU,” *Mon. Not. Roy. Astron. Soc.* **491** no. 2, (2020) 3022–3041, [arXiv:1911.03545](#) [[astro-ph.CO](#)].
- [64] O. H. E. Philcox and D. J. Eisenstein, “Computing the Small-Scale Galaxy Power Spectrum and Bispectrum in Configuration-Space,” *Mon. Not. Roy. Astron. Soc.* **492** no. 1, (2020) 1214–1242, [arXiv:1912.01010](#) [[astro-ph.CO](#)].
- [65] Y. P. Jing, “Correcting for the alias effect when measuring the power spectrum using FFT,” *Astrophys. J.* **620** (2005) 559–563, [arXiv:astro-ph/0409240](#).

- [66] K. Yamamoto, M. Nakamichi, A. Kamino, B. A. Bassett, and H. Nishioka, “A Measurement of the quadrupole power spectrum in the clustering of the 2dF QSO Survey,” *Publ. Astron. Soc. Jap.* **58** (2006) 93–102, [arXiv:astro-ph/0505115](#).
- [67] N. Hand, Y. Feng, F. Beutler, Y. Li, C. Modi, U. Seljak, and Z. Slepian, “nbodykit: an open-source, massively parallel toolkit for large-scale structure,” *Astron. J.* **156** no. 4, (2018) 160, [arXiv:1712.05834 \[astro-ph.IM\]](#).
- [68] J. Hartlap, P. Simon, and P. Schneider, “Why your model parameter confidences might be too optimistic: Unbiased estimation of the inverse covariance matrix,” *Astron. Astrophys.* **464** (2007) 399, [arXiv:astro-ph/0608064](#).
- [69] F. Lacasa, M. Aubert, P. Baratta, J. Carron, A. Gorce, S. G. Beauchamps, L. Legrand, A. Moradinezhad Dizgah, and I. Tutusaus, “Efficient computation of the super-sample covariance for stage IV galaxy surveys,” *Astron. Astrophys.* **671** (2023) A115, [arXiv:2209.14421 \[astro-ph.CO\]](#).
- [70] **Planck** Collaboration, N. Aghanim *et al.*, “Planck 2018 results. VI. Cosmological parameters,” *Astron. Astrophys.* **641** (2020) A6, [arXiv:1807.06209 \[astro-ph.CO\]](#). [Erratum: *Astron. Astrophys.* 652, C4 (2021)].
- [71] O. H. E. Philcox and M. M. Ivanov, “BOSS DR12 full-shape cosmology: Λ CDM constraints from the large-scale galaxy power spectrum and bispectrum monopole,” *Phys. Rev. D* **105** no. 4, (2022) 043517, [arXiv:2112.04515 \[astro-ph.CO\]](#).
- [72] M. M. Ivanov, O. H. E. Philcox, G. Cabass, T. Nishimichi, M. Simonović, and M. Zaldarriaga, “Cosmology with the Galaxy Bispectrum Multipoles: Optimal Estimation and Application to BOSS Data,” [arXiv:2302.04414 \[astro-ph.CO\]](#).
- [73] V. Desjacques, D. Jeong, and F. Schmidt, “Large-Scale Galaxy Bias,” *Phys. Rept.* **733** (2018) 1–193, [arXiv:1611.09787 \[astro-ph.CO\]](#).
- [74] J. Skilling, “Nested sampling for general Bayesian computation,” *Bayesian Analysis* **1** no. 4, (2006) 833–859.
- [75] W. J. Handley, M. P. Hobson, and A. N. Lasenby, “PolyChord: nested sampling for cosmology,” *Mon. Not. Roy. Astron. Soc.* **450** no. 1, (2015) L61–L65, [arXiv:1502.01856 \[astro-ph.CO\]](#).
- [76] W. J. Handley, M. P. Hobson, and A. N. Lasenby, “polychord: next-generation nested sampling,” *Mon. Not. Roy. Astron. Soc.* **453** no. 4, (2015) 4385–4399, [arXiv:1506.00171 \[astro-ph.IM\]](#).
- [77] O. H. E. Philcox, “Cosmology without window functions: Quadratic estimators for the galaxy power spectrum,” *Phys. Rev. D* **103** no. 10, (2021) 103504, [arXiv:2012.09389 \[astro-ph.CO\]](#).
- [78] O. H. E. Philcox, “Cosmology without window functions. II. Cubic estimators for the galaxy bispectrum,” *Phys. Rev. D* **104** no. 12, (2021) 123529, [arXiv:2107.06287 \[astro-ph.CO\]](#).
- [79] C. Hahn, M. Eickenberg, S. Ho, J. Hou, P. Lemos, E. Massara, C. Modi, A. Moradinezhad Dizgah, B. R.-S. Blancard, and M. M. Abidi, “SimBIG: mock challenge for a forward modeling approach to galaxy clustering,” *JCAP* **04** (2023) 010, [arXiv:2211.00660 \[astro-ph.CO\]](#).
- [80] C. Hahn, M. Eickenberg, S. Ho, J. Hou, P. Lemos, E. Massara, C. Modi,

- A. Moradinezhad Dizgah, B. R.-S. Blacard, and M. M. Abidi, “SIMBIG: A Forward Modeling Approach To Analyzing Galaxy Clustering,” [arXiv:2211.00723 \[astro-ph.CO\]](#).
- [81] Y. Kobayashi, T. Nishimichi, M. Takada, and H. Miyatake, “Full-shape cosmology analysis of the SDSS-III BOSS galaxy power spectrum using an emulator-based halo model: A 5% determination of σ_8 ,” *Phys. Rev. D* **105** no. 8, (2022) 083517, [arXiv:2110.06969 \[astro-ph.CO\]](#).
- [82] S. Yuan, L. H. Garrison, D. J. Eisenstein, and R. H. Wechsler, “Stringent σ_8 constraints from small-scale galaxy clustering using a hybrid MCMC + emulator framework,” *Mon. Not. Roy. Astron. Soc.* **515** no. 1, (2022) 871–896, [arXiv:2203.11963 \[astro-ph.CO\]](#).
- [83] C. Dvorkin *et al.*, “Machine Learning and Cosmology,” in *Snowmass 2021*. 3, 2022. [arXiv:2203.08056 \[hep-ph\]](#).
- [84] A. Lewis, A. Challinor, and A. Lasenby, “Efficient computation of CMB anisotropies in closed FRW models,” *Astrophys. J.* **538** (2000) 473–476, [arXiv:astro-ph/9911177](#).
- [85] A. Lewis, “GetDist: a Python package for analysing Monte Carlo samples,” [arXiv:1910.13970 \[astro-ph.IM\]](#).
- [86] D. J. Eisenstein and W. Hu, “Power spectra for cold dark matter and its variants,” *Astrophys. J.* **511** (1997) 5, [arXiv:astro-ph/9710252](#).
- [87] J. Hamann, S. Hannestad, J. Lesgourgues, C. Rampf, and Y. Y. Y. Wong, “Cosmological parameters from large scale structure - geometric versus shape information,” *JCAP* **07** (2010) 022, [arXiv:1003.3999 \[astro-ph.CO\]](#).
- [88] O. H. E. Philcox, M. M. Ivanov, G. Cabass, M. Simonović, M. Zaldarriaga, and T. Nishimichi, “Cosmology with the Redshift-Space Galaxy Bispectrum Monopole at One-Loop Order,” [arXiv:2206.02800 \[astro-ph.CO\]](#).
- [89] R. Scoccimarro, L. Hui, M. Manera, and K. C. Chan, “Large-scale Bias and Efficient Generation of Initial Conditions for Non-Local Primordial Non-Gaussianity,” *Phys. Rev. D* **85** (2012) 083002, [arXiv:1108.5512 \[astro-ph.CO\]](#).
- [90] W. R. Coulton, F. Villaescusa-Navarro, D. Jamieson, M. Baldi, G. Jung, D. Karagiannis, M. Liguori, L. Verde, and B. D. Wandelt, “Quijote-PNG: Simulations of Primordial Non-Gaussianity and the Information Content of the Matter Field Power Spectrum and Bispectrum,” *Astrophys. J.* **943** no. 1, (2023) 64, [arXiv:2206.01619 \[astro-ph.CO\]](#).
- [91] G. Cabass, M. M. Ivanov, O. H. E. Philcox, M. Simonovic, and M. Zaldarriaga, “Constraining Single-Field Inflation with MegaMapper,” [arXiv:2211.14899 \[astro-ph.CO\]](#).
- [92] R. Angulo, M. Fasiello, L. Senatore, and Z. Vlah, “On the Statistics of Biased Tracers in the Effective Field Theory of Large Scale Structures,” *JCAP* **09** (2015) 029, [arXiv:1503.08826 \[astro-ph.CO\]](#).
- [93] X. Chen, “Primordial Non-Gaussianities from Inflation Models,” *Adv. Astron.* **2010** (2010) 638979, [arXiv:1002.1416 \[astro-ph.CO\]](#).
- [94] M. Liguori, E. Sefusatti, J. R. Fergusson, and E. P. S. Shellard, “Primordial Non-Gaussianity and Bispectrum Measurements in the Cosmic Microwave Background and Large-Scale Structure,” *Advances in Astronomy* **2010** (Jan., 2010) 980523, [arXiv:1001.4707 \[astro-ph.CO\]](#).
- [95] R. Scoccimarro, E. Sefusatti, and M. Zaldarriaga, “Probing primordial non-Gaussianity with large - scale structure,” *Phys. Rev. D* **69** (2004) 103513, [arXiv:astro-ph/0312286](#).

- [96] N. Hand, Y. Li, Z. Slepian, and U. Seljak, “An optimal FFT-based anisotropic power spectrum estimator,” *JCAP* **07** (2017) 002, [arXiv:1704.02357](#) [[astro-ph.CO](#)].
- [97] G. D’Amico, Y. Donath, M. Lewandowski, L. Senatore, and P. Zhang, “The BOSS bispectrum analysis at one loop from the Effective Field Theory of Large-Scale Structure,” [arXiv:2206.08327](#) [[astro-ph.CO](#)].